Chapter 2

Synthesis and Study of Curcuminoid based Chiral Corands as Drug Carriers

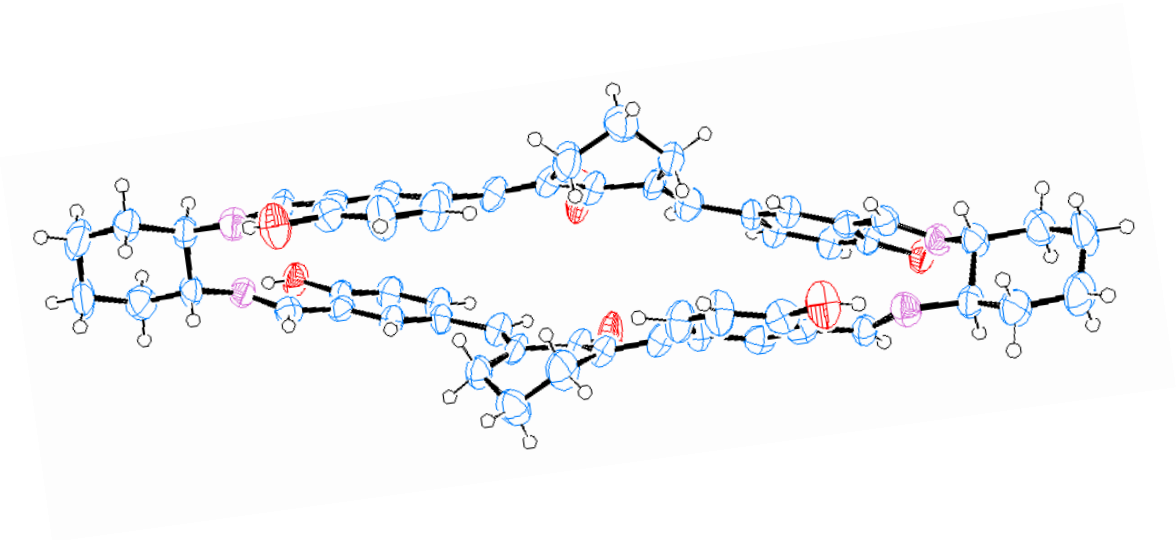

2.1. Introduction

Supramolecular Delivery Systems (SDSs), which are designed and manufactured through molecular assembly, facilitate the integration of a structural diversity and multiple functions into a single system[1]. SDSs are a highly active field of research because of their great potential in biomedical applications such as drug delivery, cellular imaging, diagnosis and release monitoring[2]. Supramolecules in the field of drug delivery systems integrate target groups and control the components to achieve targeted, controlled and specific delivery of their payloads[3]. Stereoselectivity should be taken into account when creating intelligent supramolecular drug carriers that interact with their targets. Enantioselectivity towards binding their substrates is an important characteristic of proteins. The binding affinity of a chiral drug carrier can vary between enantiomers and diastereomers[4]. Although chirality is common in biological systems, manipulating chirality in biomaterials to affect interactions with cells has just lately been investigated[5]. Drug deposition processes that rely on interactions with chiral biological macromolecules, such as active transport, binding to plasma proteins, and drug metabolism, are known to exhibit stereoselectivity. However, distinctions between enantiomer and diasteromer would be anticipated if a chiral drug carrier served as a substrate for an active transport process, with one of the stereoisomer being preferentially absorbed[6]. The previous researcher has shown that chirality affects the cellular uptake[7], cell adhesion[8], cell differentiation[9,10], protein adsorption[11,12], and cytotoxicity[13]. We also know that chiral excipients, such as natural biomolecules, are among the most widely employed chiral carriers. Chiral interactions are likely to take place and play important roles during drug delivery[14].

Unfortunately, research on enantioselective effects during drug release has been neglected. While on the other hand in the broad field of supramolecular chemistry lots of chiral macrocycles are reported till date[15-42] but the application of them as drug carriers is limited.

The most active precursor for synthesizing a chiral macrocycle is (1*R*, 2*R*)-cyclohexane-1, 2-diamine which is also a part of active pharmaceutical ingredients.

In 2018, a series of novel C-5 arylated calixsalens are reported by Petryk et. al. using the [3+3] cyclocondensation of trans (1*R*, 2*R*)-cyclohexane-1, 2-diamine with derivatives of 2-hydroxyisophthalaldehyde. When 2, 5-dimethoxybenzene groups were introduced in the calixsalen backbone, head-to-head capsule formation was observed; when 3, 5-

dimethylbenzene groups were introduced, tail-to-tail dimer formation was observed. It resulted in unique truncated tetrahedron-shaped cavity (figure 2.1)[43].

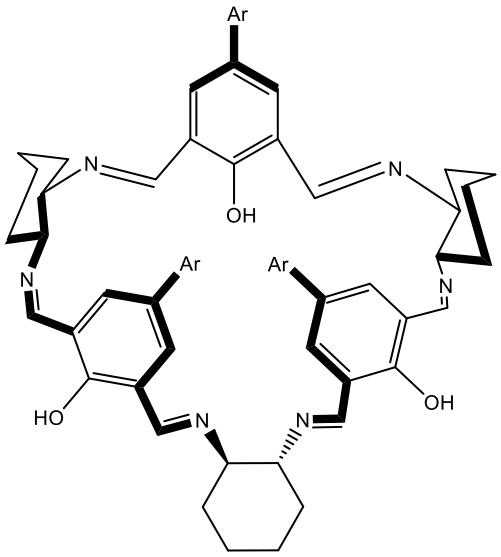

Figure. 2.1. Calixsalen molecule synthesiszed by Petryk et. al.

Following the condensation of substituted 2, 4- and 4, 6-dihydroxyisopthalaldehydes with optically pure and racemic trans (1*R*, 2*R*)-cyclohexane-1, 2-diamine, Szymkowiak et. al. produced resorcinarene-like polyimine macrocycles (resorcinsalens). They investigated the effect of structure of aldehyde, reaction conditions and the enantiomeric purity of diamine on the structure of synthesized macrocycle (figure 2.2)[44].

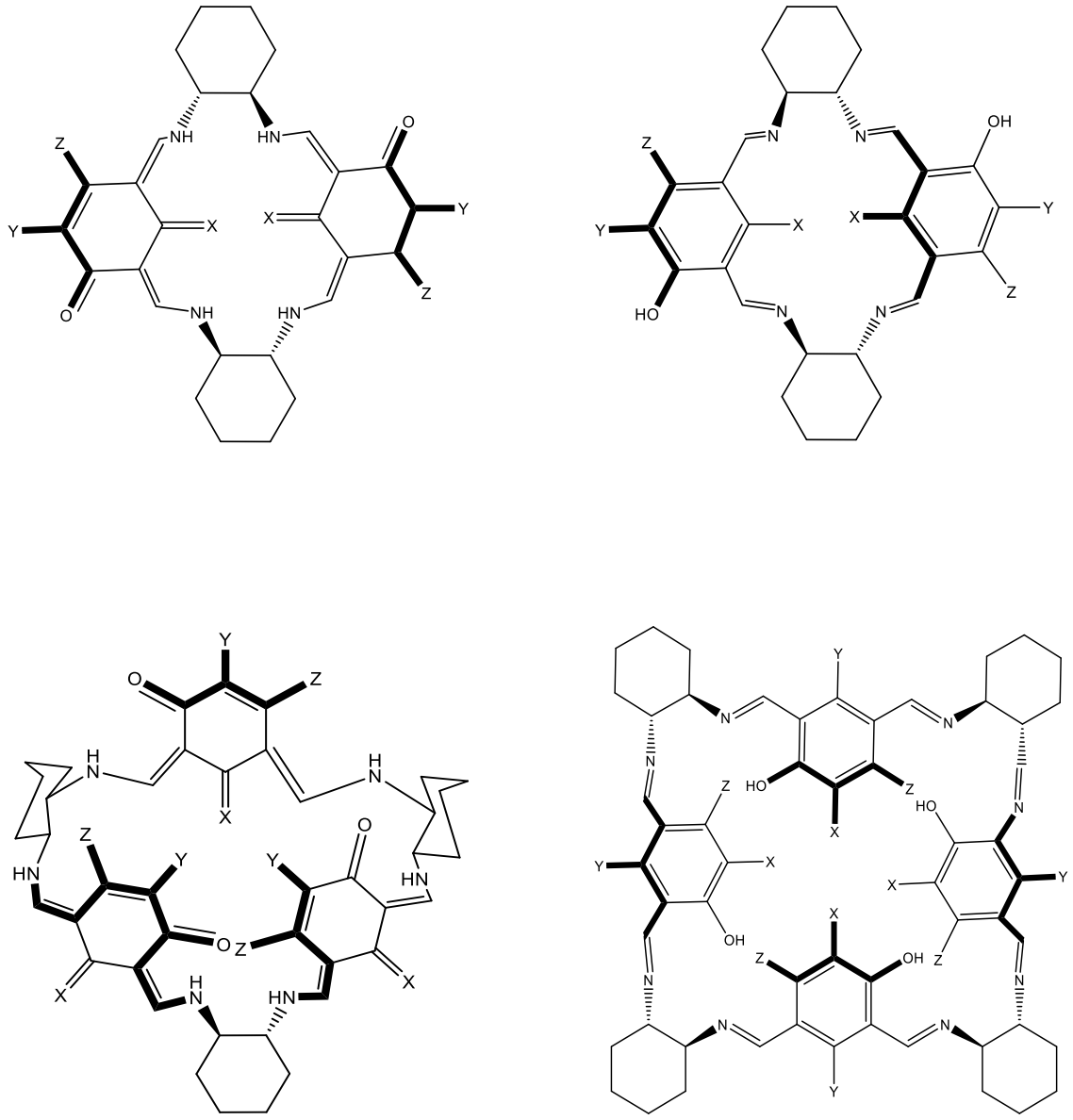

X= OH, H, CH_3.

Y= Br, Cl, C_6H_{13}, CH_3.

Z= OH, H.

Figure. 2.2. General structure of resorcinsalens synthesized by Szymkowiak et. al.

Based on [3+3] condensation, Szymkowiak et. al. also created a family of chiral, symmetrical and asymmetric, shape-persistent triangular macrocycles. The columnar arrangement of oxygenated trianglimines maintains homochirality in racemic crystals (figure 2.3)[45].

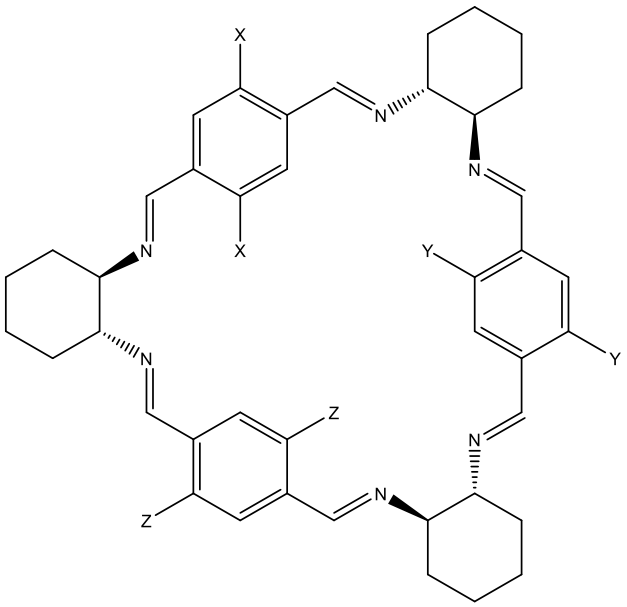

X, Y, Z= H, OH.

Figure. 2.3. General structure of trianglimines synthesized by Szymkowiak et. al.

Packowski et. al., reported a metal free synthesis of macrocycle using racemic trans -1, 2-diaminocyclohexane and 2, 6-diformyl pyridine to result in [2+2] and [4+4] cyclocondensed product. The isolated [2+2] macrocycle reacts with cadmium (II) chloride to fuse three smaller macrocyclic units into a larger [6+6] macrocycle (figure 2.4)[46].

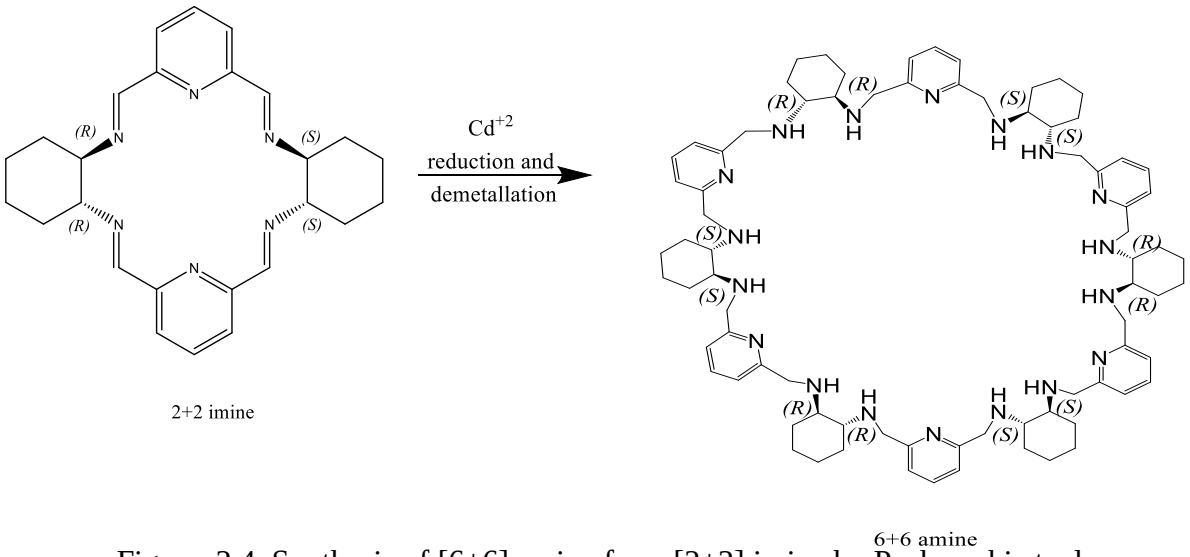

Figure. 2.4. Synthesis of [6+6] amine from [2+2] imine by Packowski et. al.

Using a dynamic combinatorial chemistry method, Frydrych et. al. created a heterochiral macrocycle via condensation reaction of 2, 6-diformylpyridine (DFP) with an equimolar mixture of opposing enantiomers of trans-1, 2-diaminocyclopentane (DACP) and trans-1, 2-diaminocyclohexane (DACH) (figure 2.5)[47].

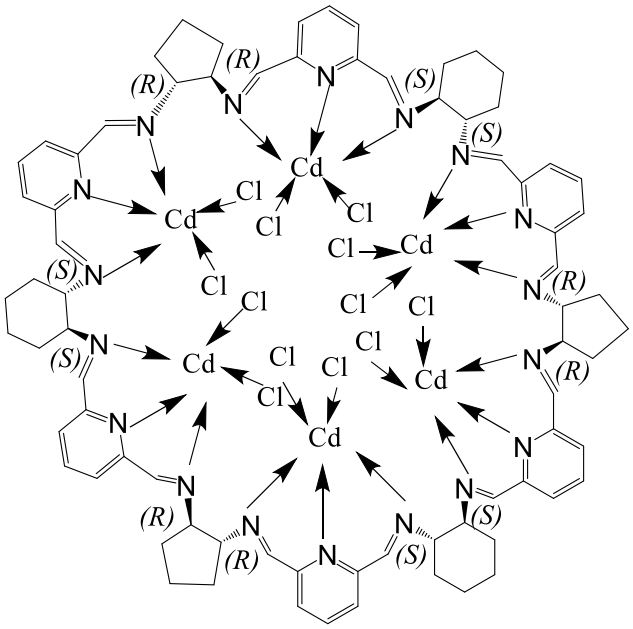

Figure. 2.5. Chiral mixed imine macrocyclic compounds synthesized from DFP and opposite enantiomers of DACP and DACH.

In order to create rhombimine, Zgrozelak used racemic bis-aldehyde and enantiopure trans (1*R*, 2*R*)-cyclohexane-1, 2-diamine. The main characteristic of the synthesis is the integration of a spirorhombimine, axially chiral surrounding quaternary carbon atom with four constitutionally identical substituents (figure 2.6)[48].

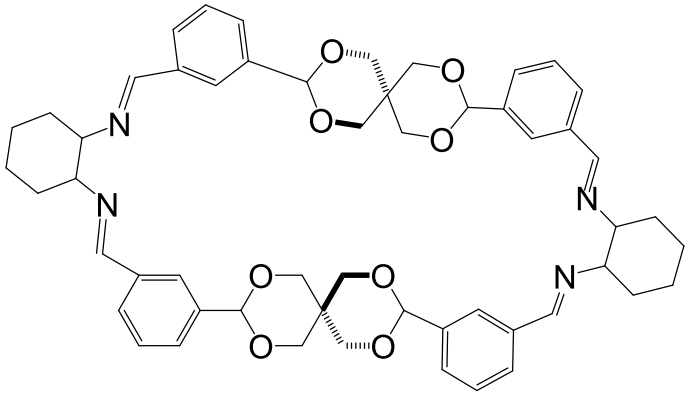

Figure. 2.6. Structure of spirorhombimine synthesized by Zgorzelak et. al.

Zgorzelak et. al. synthesized, a chiral square-shaped octaimine gigantic macrocycle under controlled conditions using inexpensive substrate trans-1, 2-diaminocyclohexane and bis-aldehyde derived from 9, 10-diphenylanthracene[49].

Fedorowicz et. al. designed and synthesised six potential diastereomers of [4+4] macrocyclic amine derived from trans-1, 2-diaminocyclopentane (DACP) and 2, 6-diformypyridine (DFP) units (figure 2.7)[50].

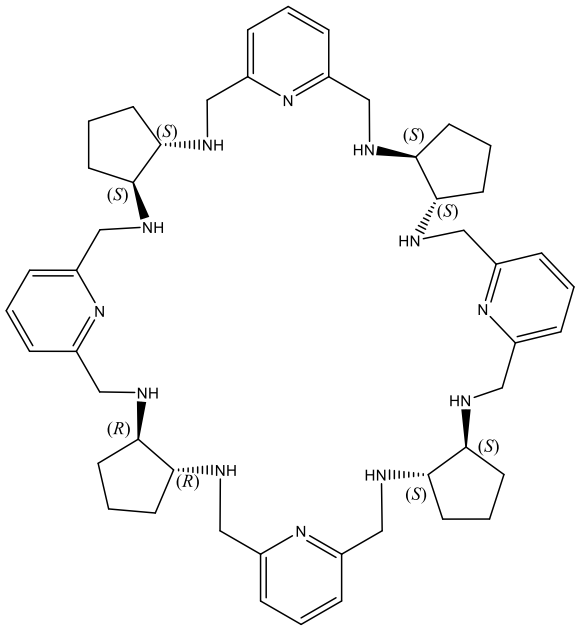

Figure. 2.7. Structure of heterochiral [4+4] amine macrocycle.

According to Janiak et. al., chiral isotrianglimines were produced by [3 + 3] cyclocondensation of (1*R*, 2*R*)-1, 2-diaminocyclohexane and derivatives of isophthalaldehyde. The conformation of individual macrocycles and their tendency to build supramolecular architectures have been influenced by the substituent's steric and electronic requirements as well as the nature of the guest molecules[51].

Desai et. al. reported the high dilution synthesis of chiral cavitands without the use of a template or metal ions using (1*R*, 2*R*)-diaminocyclohexane (DACH) and different 5, 5'-methylene-bis-salicylaldehydes and their use as selective chemo-sensors for copper and zinc ions among the first raw transition metal ions (figure 2.8)[52].

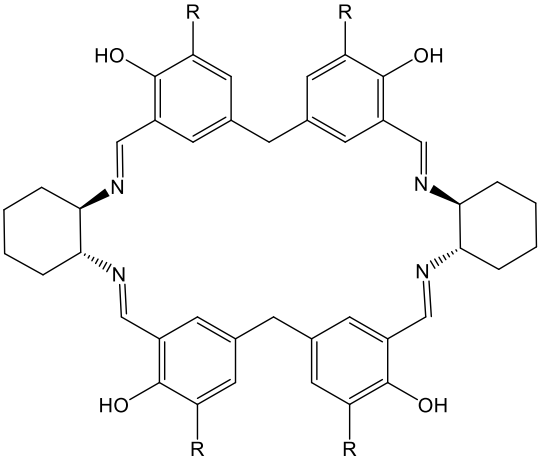

Figure. 2.8. Structure of chiral cavitand synthesized by Desai et. al.

After detailed literature review of chiral macrocycles, the following are the factors which primarily motivated us to synthesize a chiral corand molecule as a drug carrier. (1) In commercially available drugs, and particularly in those still in development, the proportion of chiral pharmaceuticals are increased. Studies in this area are still very few in number, nevertheless. (2) Studies on enantioselective release may lead to novel applications for several chiral medicines that are sold as racemic mixes. (3) Due to chiral nature of biological receptors such as human bodies and other biological receptors, chiral carriers may have enantioselective effects on achiral drugs also. Even for achiral pharmaceuticals, chirality can be used as a controlling factor to find new controlled delivery methods[53].

In the present work we have developed a drug delivery system using DACH ligand and Curcuminoid. Curcuminoid used here is synthetic analogue of Curcumin. Curcumin is polyphenolic extract of plant *Curcuma longa* (turmeric), a healthy spice from the Zingiberaceae family, has been utilized extensively for many different things[54]. Despite having several advantageous properties, curcumin has low bioavailability and low absorption due to the presence of the β-diketone moiety. The stability and solubility in water of curcumin are also lacking[55]. The replacement of β-diketone with monoketo group enhances its efficacy as well as its stability[56-63]. This modified curucminoid is further use to develop tetraiminochiralcorand as a drug carrier.

2.2. Experimental Section

2.2.1. Materials

The chemicals and solvents used in the preparation of curcuminoid based tetraiminochiralcorand were of analytical grade and purchased from Merck, Spectrochem, Loba chemicals, TCI and SRL. Chemicals were used without further purification.

2.2.2. Synthesis of 2, 6-bis ((E)-4-hydroxybenzylidene)cyclohexan-1-one[64]

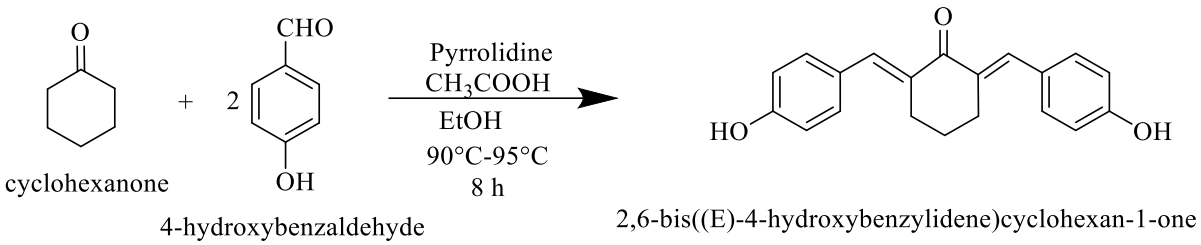

Scheme. 2.1. Synthesis of 2, 6-bis ((E)-4-hydroxybenzylidene)cyclohexan-1-one

Cyclohexanone (4.8 g, 0.049 mole) and p-hydroxybenzaldehyde (12 g, 0.098 mole) dissolved in 98 ml ethanol were placed in a 250 ml 2 neck round bottom flask equipped with condenser and guard tube. Catalytic amount of pyrrolidine (2 ml) was added and reaction mixture was refluxed at 90°C-95ºC. After refluxing for one hour, acetic acid (2 ml) was added and continued reflux for 8 hours at same temperature. Completion of reaction was confirmed by TLC. The product was filtered and washed with 100 ml distilled water. Dried under the vacuum. 8.6 g yellow free flowing solid was obtained.

Yield: 66 %

M.P.: 214 °C

^{1}HNMR: (400 MHz, DMSO-d_6): δ 10.01 (1H, s), 7.53 (1H, s), 7.41 (1H, *J* = 8.4 Hz, d), 6.84 (1H, *J* = 8.8 Hz, d), 2.85 (2H, t), 1.70 (1H, quint)

^{13}CNMR: (400 MHz, DMSO-d_6): δ 189.03, 158.79, 136.30, 133.78, 132.94, 126.92, 116.02, 28.43, 22.99.

2.2.3. Synthesis of 5, 5'-((1E, 1'E)-(2-oxocyclohexane-1, 3-diylidene)bis(methanylylidene))bis(2-hydroxybenzaldehyde)[65-68].

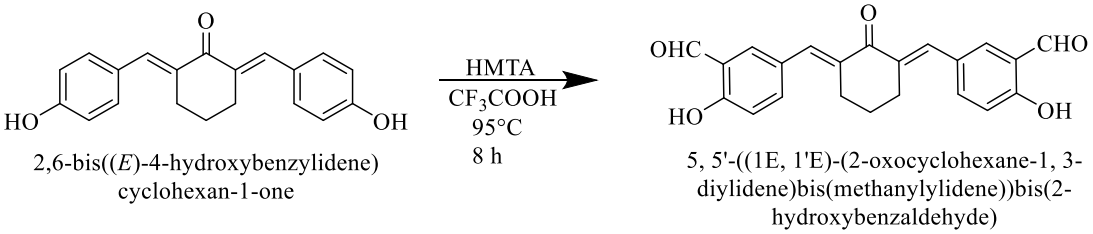

2,6-bis((*E*)-4-hydroxybenzylidene) cyclohexan-1-one

5, 5'-((1E, 1'E)-(2-oxocyclohexane-1, 3-diylidene)bis(methanylylidene))bis(2-hydroxybenzaldehyde)

Scheme. 2.2. Synthesis of bis-aldehyde.

2, 6-bis ((E)-4-hydroxybenzylidene)cyclohexan-1-one (1 g, 0.0033 moles) was dissolved in 15 ml TFA and stirred for 10 minutes at 20 ℃. HMTA (0.96 g, 0.0068 moles) was added at 20 ℃ and continued stirring for 20 minutes. The reaction mixture was refluxed for 8 hours at 95 °C. Completion of reaction was monitored by TLC. The mixture was poured in 200 ml water. The product was filtered, washed, and dried under vacuum. Product was purified using silica gel column chromatography with dichloromethane solvent.

Yield: 53%

M.P.: 176°C

FT-IR (KBr disc, cm^{-1}): 3214.61 $_{(\upsilon\text{-OH})}$, 2940.73$_{(\upsilon\text{-CH})}$, 2860.08$_{(\upsilon\text{-C=O})}$, 2833.64$_{(\upsilon\text{-C=O})}$, 2738.63$_{(\upsilon\text{-C=O})}$, 1662.51$_{(\upsilon\text{-C=O})}$, 1598.77$_{(\upsilon\text{-C=C})}$.

^{1}HNMR: (400 MHz, $CDCl_3$): δ 11.19(1H, s), 9.96(1H, s), 7.77(1H, s), 7.70(1H, *J* = 2.0 Hz, d), 7.68(1H, *J* = 2.0 Hz, d), 7.07(1H, J = 8.4 Hz, d), 2.96(2H, t), 1.87(1H, qunit).

^{13}CNMR: (400 MHz, $CDCl_3$): δ 196.47, 189.48, 161.77, 138.88, 135.92, 135.27, 135.24, 128.03, 120.47, 118.06, 28.47, 22.82.

2.2.4. Synthesis of tetraiminochiralocorand[67,68]

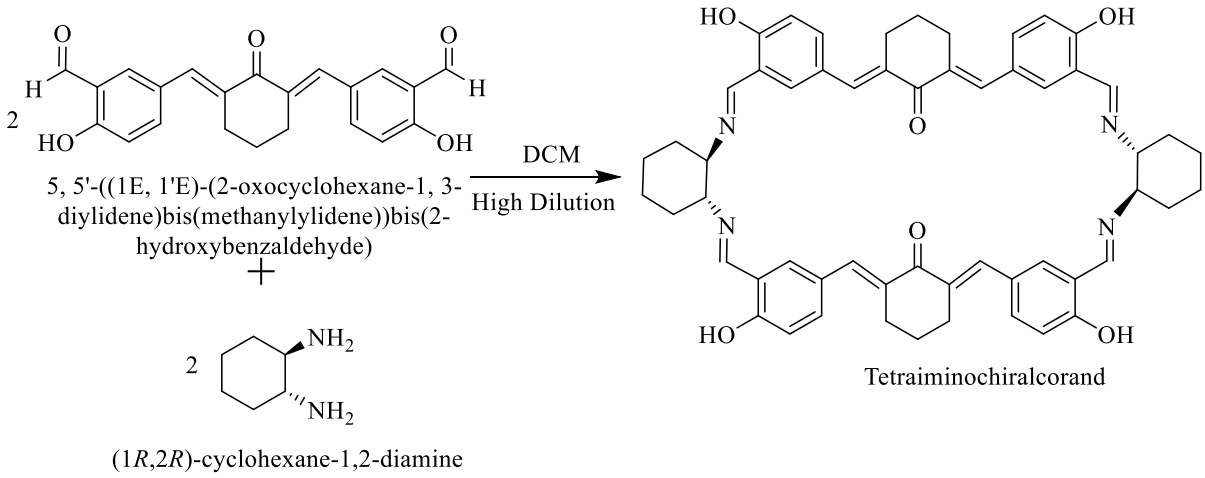

Scheme. 2.3. Synthesis of tetraiminochiralcorand.

2 L DCM (Dichloromethane) was placed in a 5 L round bottom flask. 1 g (0.0027 moles) of bis-aldehyde and 0.315 g (0.0027 moles) of (*1R, 2R*)-cyclohexane-1, 2-diamine was dissolved in 750 ml of DCM individually. Both solutions were added drop wise to mechanically stirred DCM kept in a round bottom flask over 7 to 8 hours. The reaction mixture was concentrated to 100 ml and kept for slow evaporation to obtain orange crystalline product.

Yield: 98 %

M.P.: 208°C (degraded)

FT-IR (KBr disc, cm^{-1}): 3439.39(ν_{-OH}), 2932.79 (ν_{-CHas}), 2858.95 (ν_{-CHs}), 1627.59 ($\nu_{-C=N}$), 1596.60 ($\nu_{-C=C}$).

^{1}H NMR: (400 MHz, $CDCl_3$): δ 13.89(1H, s), 7.86(1H, s), 7.43(1H, J_1 = 8.8 Hz, J_2 = 2.0 Hz, d), 7.34 (1H, s), 7.02 (1H, *J* = 8.8 Hz, d), 6.89 (1H, *J* = 2.0 Hz, d), 3.17 (1H, t), 2.58-2.51 (1H, m), 2.41-2.34 (1H, m), 2.25 (1H, d), 1.96 (1H, d), 1.89 (1H, d), 1.52 (1H, t), 1.45 (1H, t).

^{13}C NMR: (400 MHz, $CDCl_3$): δ 191.55, 166.20, 162.20, 134.92, 134.81, 134.71, 133.69, 126.66, 117.70, 117.53, 70.75, 32.09, 28.06, 24.02, 22.73.

DEPT135 NMR: (400 MHz, $CDCl_3$): δ 166.21, 134.94, 134.83, 133.71, 117.53, 70.72, 32.07, 28.07, 24.01, 22.74.

HRMS: 881.4012 [M+1] (Theoretical Mass [M+1] = 881.4200).

2.2.5. UV-Vis study

5 ml of 0.1 x 10^{-3} M solution of tetraiminochiralcorand, silvercorate, nilutamide, and inclusion complexes were prepared in DMSO and recorded UV-Vis spectra of all these solution at 26 °C.

2.2.6. NMR titration

^{1}H NMR titrations were recorded on 400 MHz Bruker instrument to study the encapsulation of nilutamide with the silvercorate. 0.6 ml of 1 x 10^{-2} M solution of nilutamide was prepared in DMSO-d_6 and placed in the NMR tube. NMR titrations were carried out by adding 15 µl, 2 x 10^{-2} M solution of silvercorate.

2.2.7. Preparation of Silver corate and encapsulation of Nilutamide

Briefly, 1 mL methanolic solution of silver nitrate 1.9 mg (0.0113 mmol) was mixed with the solution of 10 mg (0.0113 mmol) tetraiminochiralcorand in 5 ml mixture of solvents DCM: methanol::3:2. The resultant mixture was then sonicated and kneaded in dark condition. It was dried in dark to obtain a free flowing powder. 30.21 mg (0.0952 mmol) of nilutamide was dissolved in 5 ml DCM. The solution of nilutamide in DCM was added to solution of 10 mg (0.0095 mmol) of silvercorate in 5 ml DCM:methanol mixture. The resultant formulation was kneaded and dried to obtain a free flowing powder.

2.2.8. Calculation of Drug Loading (DL%) of Silver corate and Encapsulation Efficiency (EE%) of Nilutamide

The aqueous solution of 8.4 mg inclusion complex in 2 ml of conductivity water was prepared and placed into 0.1-0.5 kD MWCO, Float-A-Lyser G2, CE, Dialysis Membrane device from Repligen (Spectrum Laboratories), Inc. and subjected to dialysis in 100 ml water for 24 hours at room temperature. The concentration of free drug was determined by withdrawal of 5 ml of release medium and measuring absorption on UV-Vis spectrophotometer detection at 262 nm wavelength. The calibration plot for nilutamide was used to determine the concentration of drug released (Unbound drug) in aqueous medium. The concentration of unbound drug was subtracted from the drug added to the carrier to determine the amount of drug loaded. Using the following formulae, the drug loading (DL) and entrapment efficiency (EE) were estimated in comparison to the standard curve:

DL (%) = [($W_{Nilutamide}$ –$W_{Unbound\ Nilutamide}$) /$W_{Inclusion\ Complex}$)] x 100

EE (%) = [($W_{Nilutamide}$ – $W_{Unbound\ Nilutamide}$) /$W_{Nilutamide}$)] x 100

Where,

$W_{Nilutamide}$ = Weight of nilutamide in inclusion complex

$W_{Unbound\ Nilutamide}$ = Weight of unbound nilutamide released from inclusion complex

$W_{Inclusion\ complex}$ = Weight of inclusion complex

2.2.9. Cumulative release of Nilutamide

Dialysis bag method[69] was used to investigate the cumulative release profile of nilutamide at two different pH levels (7.4 and 5.5). Briefly, 0.1-0.5kD MWCO, Float-A-Lyser G2, CE, Dialysis Membrane device from Repligen (Spectrum Laboratories), Inc. was used for dialysis. 7.5 mg of inclusion complex was used for an experiment. 100 ml of buffer at pH 5.5 and pH 7.4 were used as release medium. A predefined volume of the release medium (5 ml) was withdrawn at regular intervals, and an equal volume of freshly made buffer was then supplied to make up for this withdrawal. Each sample was generated in triplicate, and a UV-visible spectrophotometer was used to determine the concentration of the drug released.

2.2.10. UV-VIS titration of Cis-platin and Dasatinib with Tetraiminochiralcorand

5 ml of 1 x 10^{-5} M solution of tetraiminochiralcorand was prepared in DMSO and placed 2 ml into cuvette. 2 ml of 1 x 10^{-3} M solution of cis-platin and dasatinib were prepared in DMSO. UV-Vis titrations were carried out by adding 2 µl, 1 x 10^{-3} M solution of cis-platin upto 1 equivalent of tetraiminochiralcorand then further titrated this solution by adding 2 µl, 1 x 10^{-3} M dasatinib.

2.2.11. Encapsulation of Cis-platin and Dasatinib with Tetraiminochiralcorand

The kneading approach was used to create inclusion complexes of tetraiminochiralcorand, cis-platin and dasatinib in a 1:1:10 molar ratio. In a nutshell, 2 mg (0.00227 mmol) of tetraiminochiralcorand, 0.6 mg (0.00227 mmol) of cis-platin and 11.09 mg (0.0227 mmol) of dasatinib for 1:1:10 were weighed. Their mixture was then pulverised in an agate mortar and then triturated with methanol:dichloromethane until it formed a homogenous paste. A suitable amount of solvent was added to the paste during the 45-minute kneading procedure in order to retain the paste's consistency. The finished product was dried for 24 hours at room temperature.

2.2.12. Calculation of Drug Loading (DL%) of Tetraiminochiralcorate and Encapsulation Efficiency (EE%) of Dasatinib

The aqueous solution of inclusion complex of 7.3 mg in 2 ml was prepared and placed into 0.1-0.5kD MWCO, Float-A-Lyser G2, CE, Dialysis Membrane device from Repligen (Spectrum Laboratories), Inc. and subjected to dialysis in 100 ml water for 24 hours at room temperature. The concentration of free drug was determined by withdrawal of 5 ml of release medium and measuring absorption at 325 nm on UV-spectrophotmeter. The calibration plot for dasatinib was used to determine the concentration of drug released (Unbound drug) in aqueous medium. The concentration of unbound drug was subtracted from the drug added to the carrier to determine the amount of drug loaded. Using the following formulae, the drug loading (DL) and entrapment efficiency (EE) were estimated in comparison to the standard curve:

$$DL\ (\%) = [(W_{Dasatinib} - W_{Unbound\ Dasatinib}) / W_{Inclusion\ complex})] \times 100$$

$$EE\ (\%) = [(W_{Dasatinib} - W_{Unbound\ Dasatinib}) / W_{Dasatinib})] \times 100$$

Where,

$W_{Dasatinib}$ = Weight of dasatinib in inclusion complex

$W_{Unbound\ Dasatinib}$ = Weight of unbound dasatinib released from inclusion complex

$W_{Inclusion\ complex}$ = Weight of inclusion complex

2.2.13. Cumulative release of Dasatinib

Dialysis bag method[69] was used to investigate the in vitro release profile of dasatinib at two different pH levels (7.4 and 5.5). Briefly, 0.1-0.5kD MWCO, Float-A-Lyser G2, CE, Dialysis Membrane device from Repligen (Spectrum Laboratories), Inc. was used for dialysis. 2 ml aqueous solution of 5.1 mg of inclusion complex was used for the experiment. 100 ml of buffer at pH 5.5 and pH 7.4 were used as release medium. A predefined volume of the release medium (5 ml) was withdrawn at regular intervals, and an equal volume of freshly made buffer was then supplied to make up for this withdrawal. Each sample was generated in triplicate, and a UV-visible spectrophotometer was used to determine the concentration of the drug released.

2.2.14. Cell line and culture condition

The MDA-MB-231 were procured from the National Centre of Cell Sciences, Pune and cultured in Leibovitz-15 (L-15) medium supplemented with 10% v/v heat-inactive foetal bovine serum (FBS) (HiMedia), 100 I.U./ml penicillin-streptomycin solution at 37°C and in a humidified atmosphere of 5% CO_2 in the air. The cell viability of the cells was measured with the staining of the cells with 0.25% trypan blue dye and counted in a haemocytometer under an inverted microscope.

2.2.15. Cell Cytotoxicity Assay

In 96-well plates (1×10^5 cells/ml) were seeded (100 µL/well) and incubated for 24 hours (cell recovery and attachment). The synthesized complexes, and the negative control substance dimethyl sulfoxide (DMSO) 0.2% were added to the healthy plates and again incubated for 24 hours. The healthy plates were then incubated with 10 µl of 3-(4,5-Dimethylthiazol-2-yl)-2,5-Diphenyltetrazolium Bromide (MTT) (5 mg/ml stock). MTT was removed after the 4-hour incubation period, and 100 µl of DMSO was added to dissolve the formazan crystals. The concentration was measured at 490 nm in a microplate reader, and the findings were displayed as a percentage inhibition (50% inhibition).

2.2.16. Characterization Method

FT-IR studies of all compounds were performed on Bruker Alpha FT-IR spectrometer in solid state as KBr pellets. UV-visible Spectrophotometer experiments were performed on Perkin Elmer Lambda 35 Spectrophotometer, Inc, MA, USA. NMR data was recorded on Bruker AVANCE, 400 MHz spectrometer in $CDCl_3$ and DMSO-d_6, with TMS as internal standard. An Xcalibur, EOS, Gemini diffractometer was used to acquire diffraction data for all of the synthesized compounds using graphite monochromatic Mo Kα radiation (0.71073). The Olex 2 [70] software and the ShelXL[71] refinement package were used to solve and refine all structures. MERCURY was used to create the graphics (version 3.9). Direct approaches were used to solve all structures, which were then refined in a regular way. Non-hydrogen atoms were treated anisotropically in all circumstances. The thermogram were investigated by differential scanning calorimeter (DSC) using a Perkin Elmer Thermal Analyzer with heating and cooling rate 10 °C min^{-1}.

2.3. Result and discussion

Initial studies on several curuminoid-based salen compounds revealed that the addition of an alicyclic group improves their effectiveness against both cancer and microbes. Precisely, the curcuminoids with cyclohexyl imino groups showed superior efficacy[65]. Taking this into consideration, we created the curcuminoid based macrocycle by keeping the cyclohexyl moiety intact to achieve the best anticancer activity.

With the aim to synthesize a drug carrier with capabilities of pH triggered drug release, we synthesized curcuminoid based chiral corand in three steps. In first step we have designed monoketo curcumin analogous bishydroxybenzylidene cyclohexanone. The enolization and chelating properties of β-diketo group of curcumin is known to cause structural instability, resulting in a decreased pharmacoprofile. We replaced the β-diketo group with a mono keto group (cyclohexanone), in order to increase the efficacy and bioavailability of curcuminoid (figure 2.9).

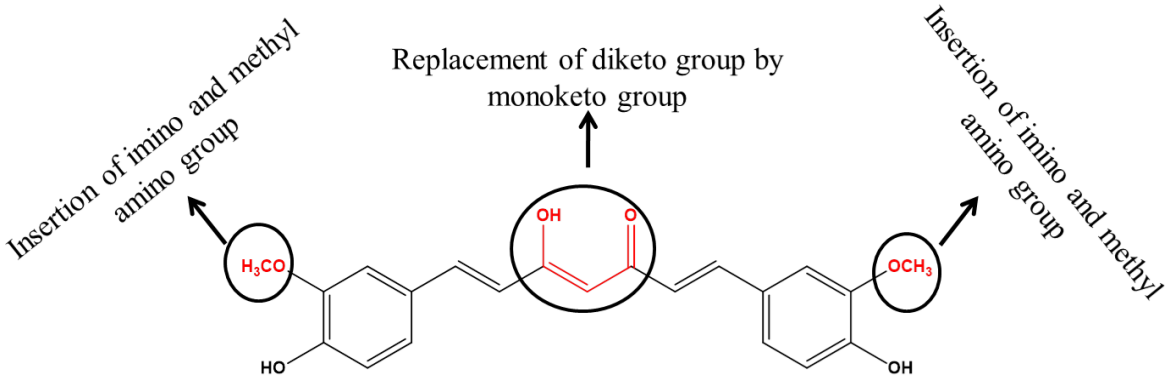

Figure. 2.9. Proposed modification in the structure of Curcumin to increase its bioavailability and aqueous solubility.

We have used the previously published protocol for synthesis of bis-hydroxybenzylidene cyclohexanone via stork-enamine reaction[64]. The p-hydroxy benzaldehyde was reacted with cyclohexanone in ethanol using pyrrolidine and acetic acid (scheme 2.1)[65]. The synthesized compound was characterized by ^{1}H NMR and ^{13}C NMR techniques (spectrum 2.1 and 2.2). In

the ^{1}H NMR spectrum of bis-hydroxybenzylidene cyclohexanone (spectrum 2.1), the singlet at 10.01 ppm corresponds to the phenolic -OH group. The vinylic hydrogen of the chalcone moiety is responsible for the singlet at 7.53 ppm. The aromatic protons appear as a doublet at 7.41 ppm and 6.84 ppm suggesting a para substituted molecule, with a coupling constant of 8.4 and 8.8, respectively. A triplet and a quintet of methylene groups of the cyclohexanone molecule appears in an aliphatic region at 2.85 ppm and 1.70 ppm. ^{13}C NMR spectrum of bis-benzylidene cyclohexanone (spectrum 2.2) showed total 9 peaks which confirmed its symmetrical structure.

Bis-benzylidene cyclohexanone was further employed for formylation on the ortho position of the –OH group of the phenyl ring without any additional purification. The bis-formylation was performed via modified duff reaction by addition of HMTA to the substrate in TFA at 0-5 ̊C followed by the reflux at 90-95 °C to obtain the bis-aldehyde (figure 2.10) in a moderate yield (scheme 2.2)[65-68].

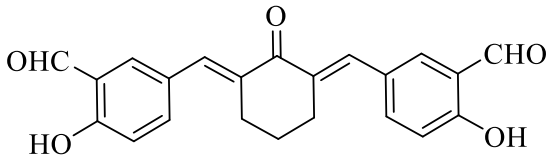

5, 5'-((1E, 1'E)-(2-oxocyclohexane-1, 3-diylidene)bis(methanylylidene))bis(2-hydroxybenzaldehyde)

Figure. 2.10. Structure of bis-aldehyde.

FT-IR spectrum of bis-aldehyde (spectrum 2.3) showed that –OH stretching band appeared at 3214.61 cm^{-1}. The –C=O bond of aldehyde functionality showed the stretching band at 1662.51 cm^{-1} while the –C=C- of alkene group of chalcone moiety showed stretching band at 1598.77 cm^{-1}. ^{1}H NMR and ^{13}C NMR spectroscopy are being used to identify bis-aldehyde. Due to hydrogen bonding with the carbonyl carbon of the aldehyde group, the peak corresponding to the -OH group shifts from 10.01 ppm (spectrum 2.1) to 11.19 ppm (bis-aldehyde) (spectrum 2.4). At 9.96 ppm, a new singlet is seen, which can be attributed to formyl hydrogen. The vinylic hydrogen of the chalcone moiety can be attributed to the singlet at 7.77 ppm. The peak corresponding to aromatic protons ortho to aldehyde appeared as a doublet at 7.70 ppm with coupling constant of 2.0 Hz and the aromatic proton para to aldehyde group also appeared as a doublet at 7.68 ppm with a coupling constant of 2.0 Hz. At 7.07 ppm, the aromatic proton ortho

to -OH group appeared as a doublet with a coupling constant of 8.4 Hz. In the aliphatic region a triplet and a quintet of methylene groups of the cyclohexanone molecule appears at 2.96 ppm and 1.87 ppm. ^{13}C NMR spectrum of bis-aldehyde (spectrum 2.5) showed total 12 peaks which confirmed the bis-formylation of bis-benzylidene cyclohexanone.

Crystal of bis-aldehyde was grown in DCM using slow evaporation method. It crystallized in monoclinic crystal system with the space group ***P*** 2_1 / *c* (figure. 2.11) (table 2.1)[65].

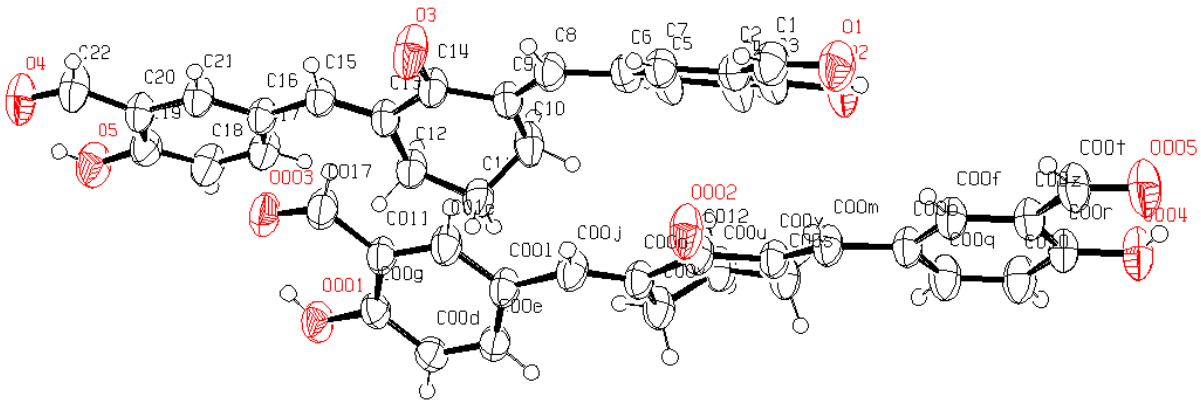

Figure. 2.11. ORTEP diagram of bis-aldehyde.

Empirical formula	C_{22} H_{18} O_5
Temperature (K)	293
Crystal system	monoclinic
Space group	$P2_1/c$
α (Å)	13.8829(9)
b (Å)	12.9132(9)
c (Å)	19.7175(15)
α (°)	90
β (°)	104.143(3)
γ (°)	90
Volume (Å ^{3})	3427.66(4)
Z	4
CCDC reference number	2174973

Table. 2.1. Crystal data of bis-aldehyde.

Classic intramolecular hydrogen-bonding interactions are seen between phenolic hydrogen and aldehyde group of bis-benzaldehyde. The phenolic –OH group serves as the hydrogen bond donor, whereas the oxygen atom of the aldehyde group serves as the hydrogen bond acceptor. Intrermolecular soft interactions between molecules are responsible for three-dimensional packing. Dimer of bis-aldehyde is held by intermolecular C-H-----π interactions between C11 atom of cyclohexanone ring of one molecule and the aromatic ring of the other molecule (figure 2.11). In the third step we carried out the macrocyclisation under high dilution conditions. Excess solvent and low concentration of reactants at a given time facilitated the intramolecular cyclisation and avoided the polymer generation.

Uses of dichloromethane as a solvent resulted in successful synthesis of such macrocycle under high dilution conditions. By using a high dilution method in dichloromethane, the synthesised bis-aldehyde and (1*R*, 2*R*)-cyclohexane-1, 2-diamine were combined to create the tetraiminochiralcorand (scheme 2.3)[67,68].

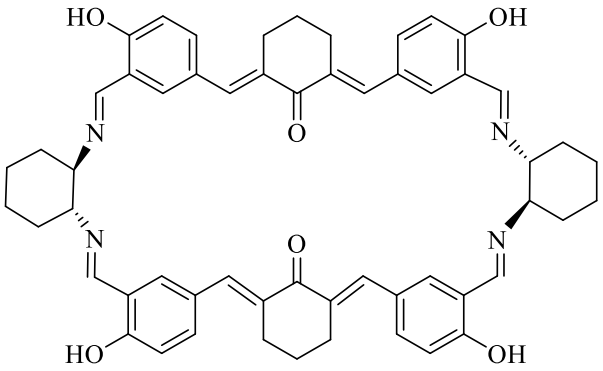

Figure. 2.12. Structure of tetraiminochiralcorand

The [2+2] cyclocondensation was observed in the formation of macrocyclic tetraiminochiralcorand with 98 % yield (figure 2.12). The tetraiminochiralcorand was characterized by FT-IR, ^{1}H NMR, ^{13}C NMR, DEPT135, HRMS, and SC-XRD techniques.

As discussed earlier, the phenolic –OH group of bis-aldehyde appeared at 3214.61 cm^{-1} (spectrum 2.3) which shifted to 3439.39 cm^{-1} (spectrum 2.6) after the formation of imine bonds in the FT-IR spectrum of tetraiminochiralcorand, while a new stretching band of imine functionality appears at 1627.59 cm^{-1}. The asymmetric stretching of $–CH_2$ was observed at

2932.79 and symmetric stretching of $–CH_2$ was observed at 2835.95 cm^{-1}. The asymmetrical alkene group showed stretching near at 1596.60 cm^{-1} due to the extended conjugation.

A symmetrical tetraiminochiralcorand structure was evident in the ^1H NMR spectrum (spectrum 2.7). A new peak of imine proton is generated at 7.86 ppm (spectrum 2.7) and the peak of aldehydic proton at 9.95 ppm (spectrum 2.4) is vanished. The proton of the phenolic hydroxyl group moved downfield to 13.89 ppm due to hydrogen bonding interaction with imine moiety. In aromatic region a double doublet is observed at 7.43 ppm with coupling constant 8.8 Hz and 2.0 Hz corresponds to an aromatic proton para to imino group indicating ortho and meta coupling respectively. A doublet at 7.02 ppm with coupling constant 8.8 Hz corresponds to aromatic proton meta to imine group and a doublet at 6.89 ppm with coupling constant 2.0 Hz corresponds to aromatic proton ortho to imino group. A singlet of a vinylic proton attached to the carbon containing aromatic ring is observed at 7.34 ppm. A triplet at 3.17 ppm corresponds to proton attached to carbon of cyclohexyl moiety containing imino group. The methylene protons of cyclohexanone moiety showed a multiplet at 2.58–2.51 ppm and a triplet at 1.45 ppm while the methylene proton of cyclohexyl group showed doublets at 2.25 ppm, 1.96 ppm, 1.89 ppm and a triplet at 1.52 ppm.

The symmetrical structure of tetraiminochiralcorand is represented by the 15-peak in ^{13}C NMR (spectrum 2.8) and 10 peaks in DEPT135 spectrum (spectrum 2.9). The DEPT135 spectrum of tetraiminochiralcorand showed 4 negative peaks due to methylene carbon and 6 positive peaks due to methine carbon.

The [2+2] cyclocondensation was confirmed by the HRMS [M+1] peak was observed at 881.4012 m/z which is in well accordance to the calculated value (spectrum 2.10).

The structure of chiral corand was further supported by SC-XRD analysis. Dichloromethane was slowly evaporated in order to crystallise the chiral corand. The structure analysis showed that two bis-benzaldehyde moiety joined with two moiety of (1*R*, 2*R*)-cyclohexane-1, 2-diamine via an imine linkage and thus produced an oval cavity with the dimension of 6.890 Å x 18.289 Å (figure 2.13). The C=N bond has a bond length of roughly 1.27 Å, which is the average bond length for imine bonds.

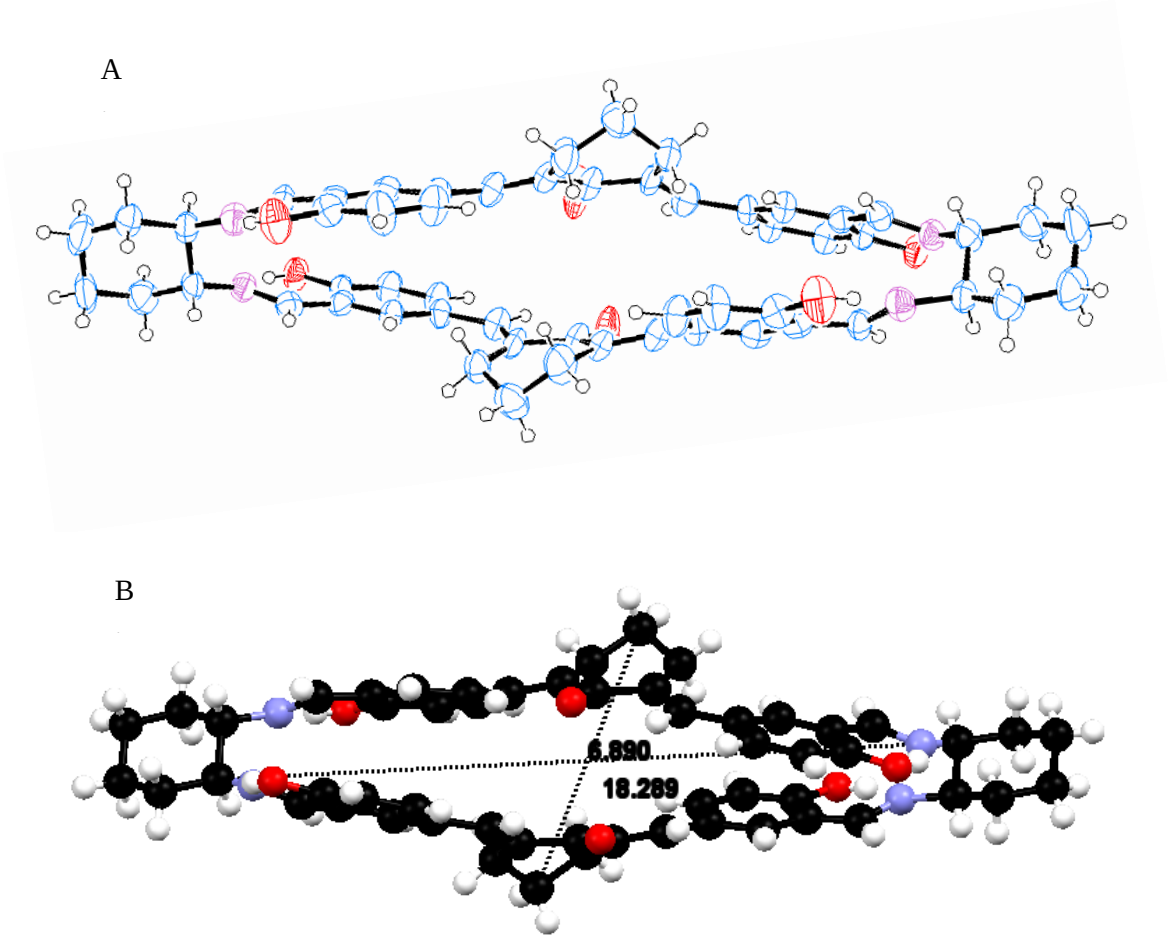

Figure. 2.13 A). ORTEP diagram of Tetraiminochiralcorand, B) Intrinsic cavity dimension of Teraiminochiralcorand.

Empirical formula	$C_{56}\ H_{56}\ N_4\ O_6$
Temperature (K)	293
Crystal system	Orthorhombic
Space group	$C222_1$
a (Å)	10.7645(11)
b (Å)	29.913(3)
c (Å)	16.626(2)
α (°)	90
β (°)	90
γ (°)	90
Volume ($Å^3$)	5353.55
Z	4
CCDC reference number	2289313

Table. 2.2. Crystal data of Tetraiminochiralcorand.

The tetraiminochiralcorand crystallises in orthorhombic crystal system with $C222_1$ chiral space group and the asymmetric unit contains half unit of macrocycle (table 2.2). Due to formation of di-equatorial bond with (1*R*, 2*R*)-cyclohexane-1, 2-diamine both the half unit of macrocycle arrange in swirl shape (figure 2.13). This swirl shape of macrocycle helps to create two separate binding pockets in the macrocycle. Four phenolic moieties are present in 1, 2-dialternate orientations where -OH groups points upward and downward alternatively constituting the wall of the cavity and making four intramolecular hydrogen bonding with the imine nitrogens. Due to the ring strain in the cyclohexanone ring, it oriented in half chair form. The width of cavity of tetraiminochiralcorand is found to be slightly larger due to the disorientation of cyclohexanone ring.

A.

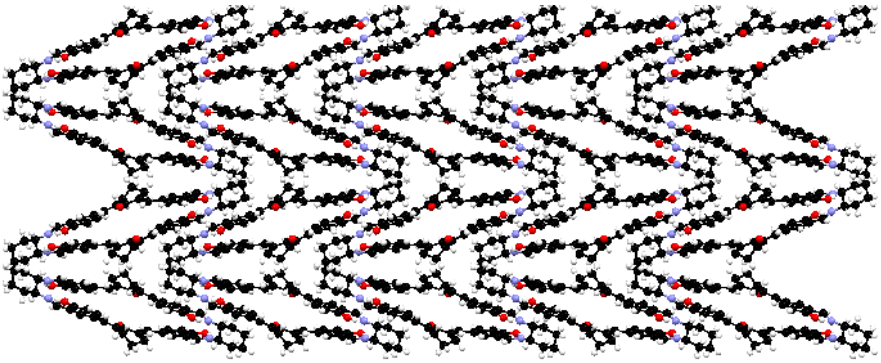

B.

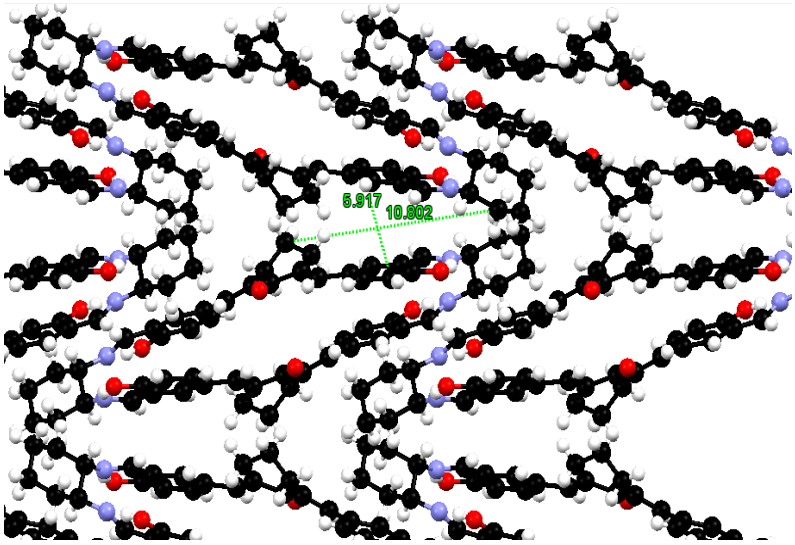

Figure. 2.14. A) Packing of Tetraiminochiralcorand along ‘a’ axis. B) Extrinsic cavity dimension of Tetraiminochiralcorand.

The edge to edge packing mode of macrocycle shows that the two tetraiminochiralcorands stack over each other which resembles an array of letter "A" (figure 2.14 A). The extrinsic cavity provides the extra compartment to entrap the high amount of guest molecule. The diameter of extrinsic cavity is around 5.917 Å X 10.302 Å (figure 2.14). This packing reveals the higher loading efficiency of guest molecule. The functional group of tetraiminochiralcorand such as imine, hydroxyl and ketone group are oriented on the periphery of the tetraiminochiralcorand which helps to hold the guest molecules.

Application of tetraiminochiralcorand as drug carrier

The tetraiminochiralcorand is explored for its application as a drug carrier. In order to do so we propose two combinatorial systems as follows:

A. Ag^+ and Nilutamide, B. Cis-platin and Dasatinib

A. Encapsulation of Ag^+ and Nilutamide in Tetraiminochiralcorand

In order to develop the immunotherapeutic system we chose the BCS class II drug Nilutamide (Nt). Nt is an antiandrogen drug used in androgen-deprivation therapy (ADT)[72]. It has been demonstrated that androgens cause proliferative alterations in breast tissue and encourage the growth of cancer cell lines in cases of breast cancer. It is well documented that the presence of androgens (DHT and non-metabolized synthetic mibolerone) stimulated the growth of MDA-MB-231 (ER-negative/AR-positive) cells[73]. We used Nilutamide with an immunomodulator Ag^+ and developed a combinatorial therapy with the tetraiminochiralcorand based drug carrier. The silver corates were synthesized via kneading approach under dark condition using tetraiminochiralcorand and silver nitrate. The silver corate was further loaded with nilutamide using kneading method to generate an inclusion complex of silver and nilutamide with tetraiminochiralcorand.

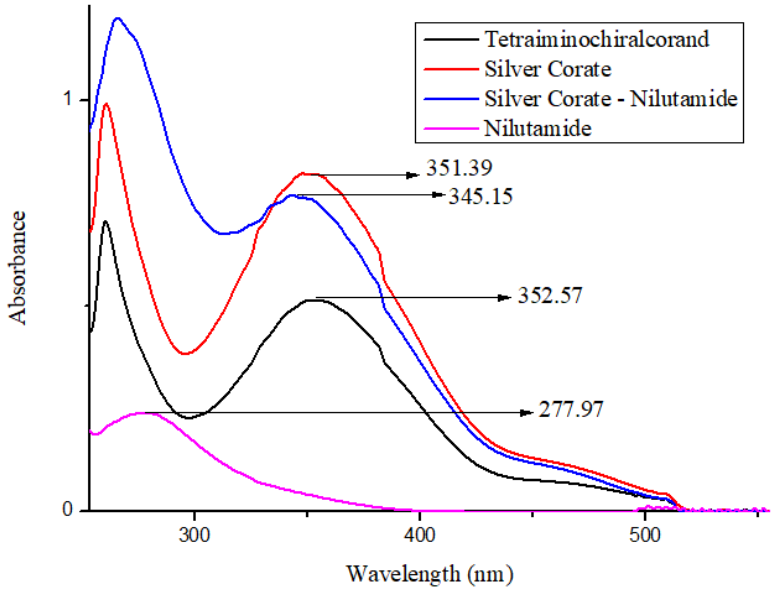

Figure. 2.15. UV-Vis absorption spectra of tetraiminochiralcorand, silver corate, nilutamide loaded silver corate and nilutamide.

The host-guest inclusion can be studied by UV-Vis spectroscopy. A hypsochromic shift from 352 nm to 351 nm with marked increase in the intensity was observed in the absorption maximum of silver corate due to n-π^* transition, suggesting encapsulation of silver by tetraiminochiralcorand while, the encapsulation of Nt by silver corate decreased the absorption intensity slightly with hypsochromic shifting from 351 nm to 345 nm (figure 2.15). These changes in the absorption band indicates the formation of inclusion complex of silver and Nt together with tetraiminochiralcorand.

The inclusion complexes are further characterized by FT-IR technique. When silver ion binds with the tetraiminochiralcorand the -C=N stretching shifted due to the participation of imine nitrogen into the coordination with silver ion, so it shifted from 1627 cm^{-1} (spectrum 2.6) to 1631 cm^{-1} (spectrum 2.11). Similarly the oxygen of –OH group of tetraiminochiralcorand also participated in the coordination to silver ion shifted from 3439 cm^{-1} (spectrum 2.6) to 3441 cm^{-1} (spectrum 2.11).

The encapsulation of Nt within silvercorate affects the interaction of silver ion with tetraiminochiralcorand. The Nt has five-membered lactum ring which showed its characteristic stretching at 1725 cm^{-1} (spectrum 2.13) which shifted to 1726 cm^{-1} (spectrum 2.12) after getting encapsulated within silver corate. This might be due to the –NH group of lactum ring being coordinated with silver ion. This newly generated non covalent interaction affects the

interaction between the–OH group of tetraiminochiralcorand and silver ion resulting in a shift from 3441 cm^{-1} (spectrum 2.11) to 3433 cm^{-1} (spectrum 2.12).

In order to explore the binding modes of Nt with silvercorate a ^{1}H NMR titration was performed in DMSO-d_6 with a constant concentration of Nt and increasing concentration of silvercorate.

The protons of Nt gives four signals in aromatic region and one in aliphatic region which can be assigned according to the literature. The amide proton of lactum ring of Nt appears at 8.825 ppm, aromatic proton ortho to nitro group appears at 8.328 ppm, aromatic proton ortho to CF_3 group appears at 8.215 ppm and the aromatic proton para to CF_3 group appears at 8.081 ppm. The aliphatic proton of Nt appears at 1.437 ppm (spectrum 2.14).

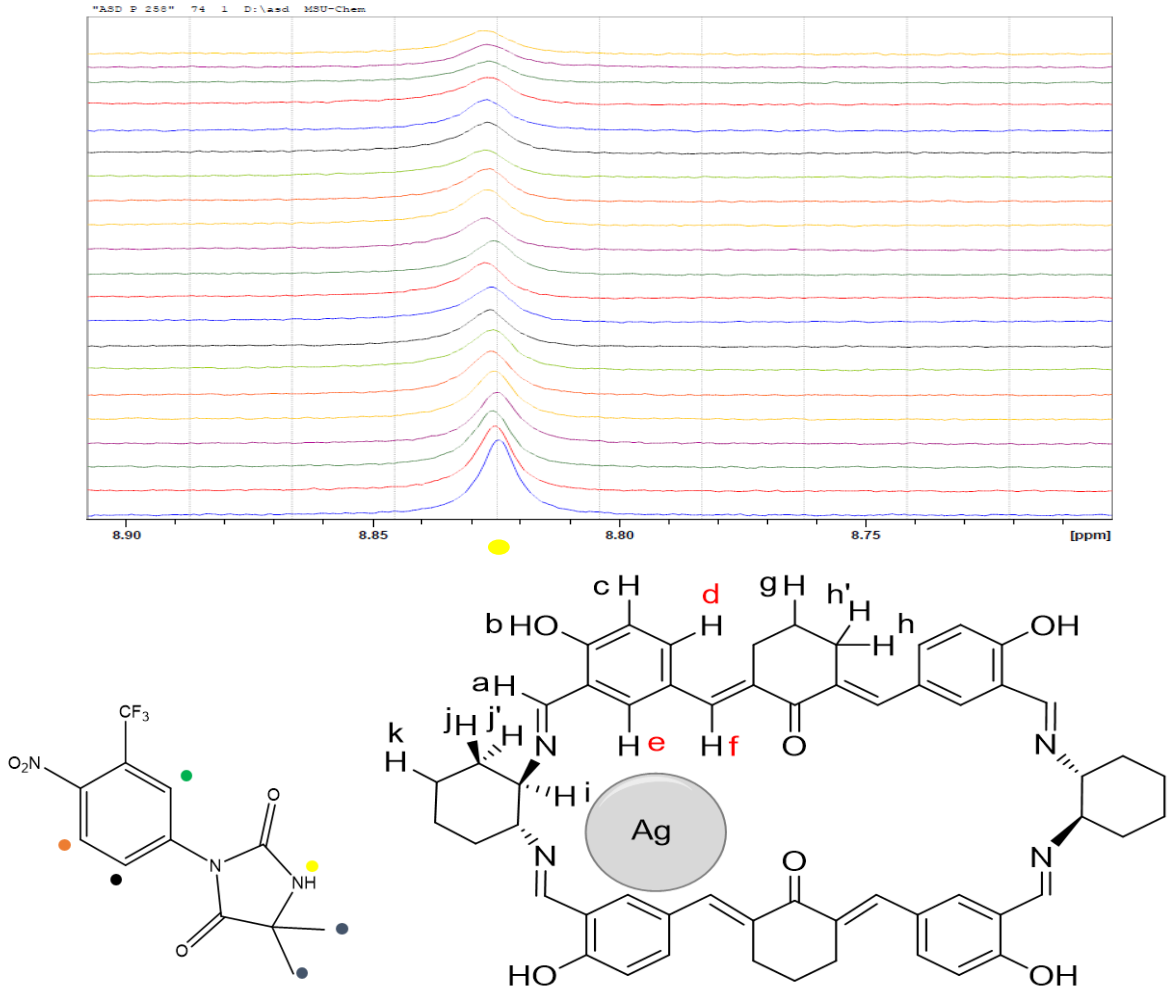

Figure. 2.16. Proton of lactum ring of Nt showed shifting in ^{1}H NMR titration.

Encapsulation of Nt in silver corate showed the chemical shift of its own proton. The amide proton of lactum ring of Nt showed the shifting from 8.825 ppm to 8.828 ppm (figure 2.16) after encapsulation into silver corate.

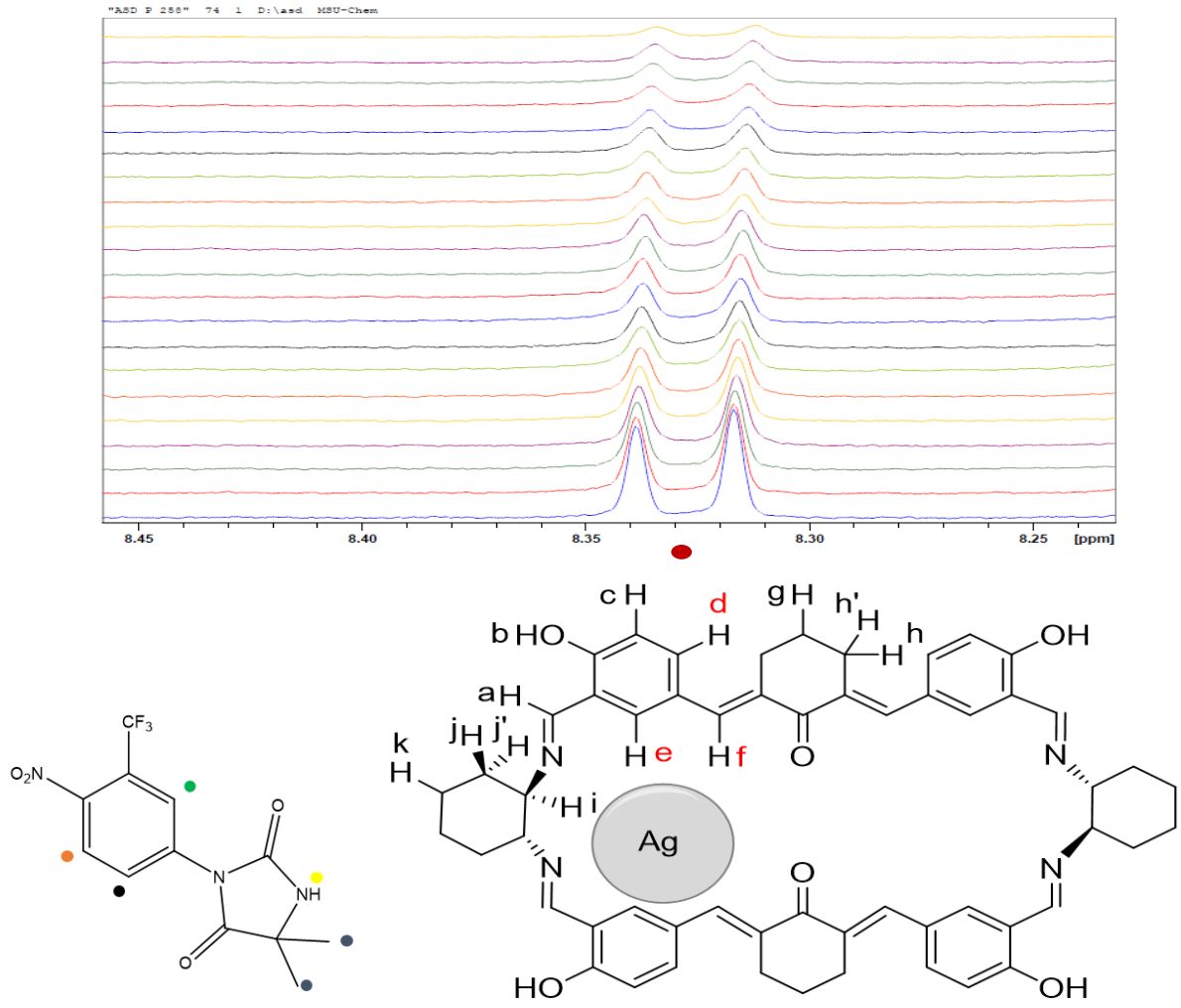

Figure. 2.17. Aromatic proton ortho to nitro group of Nt showed shifting in ^{1}H NMR titration.

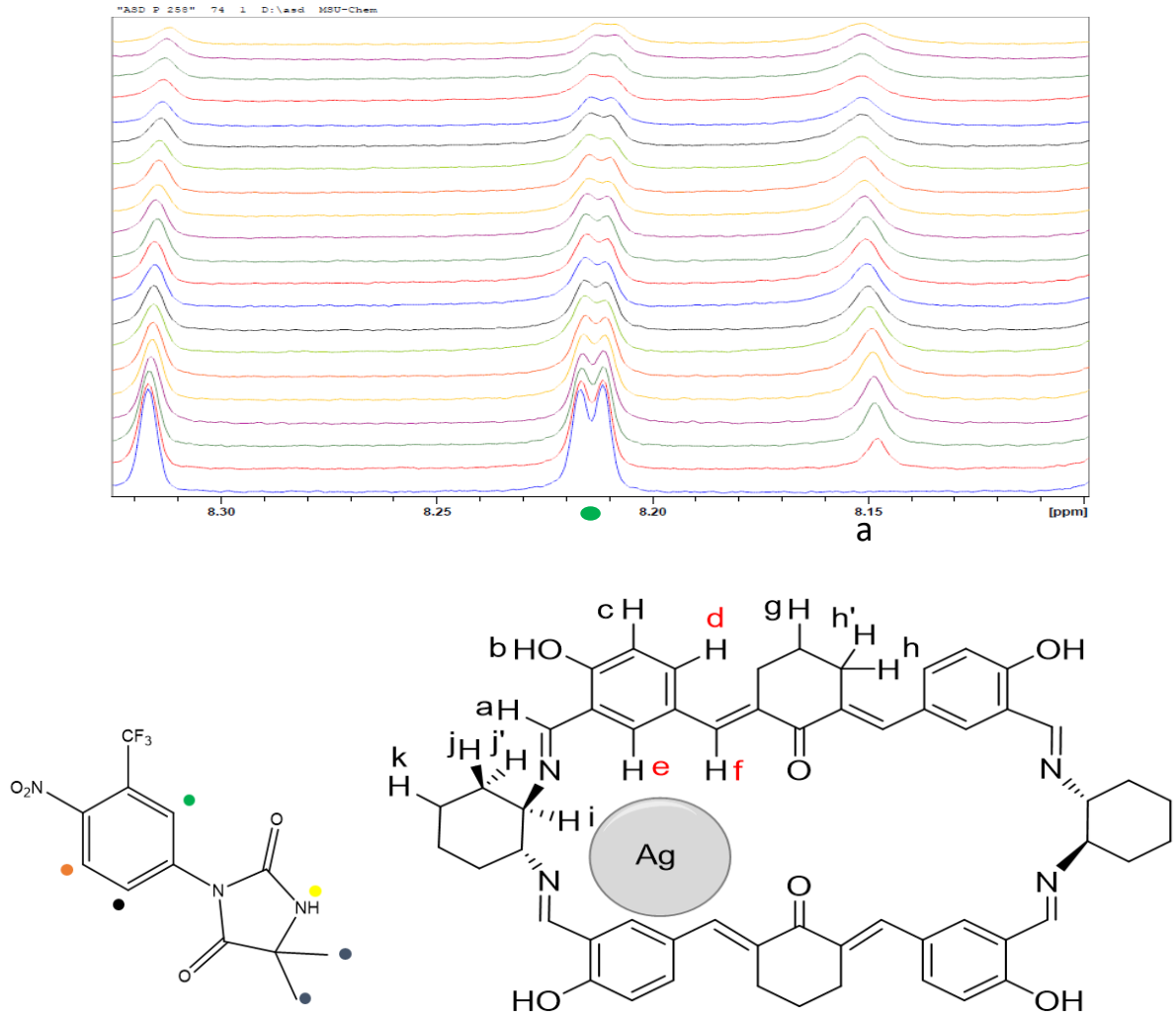

Figure. 2.18. Aromatic proton ortho to CF_3 group of Nt showed shifting in ^1H NMR titration.

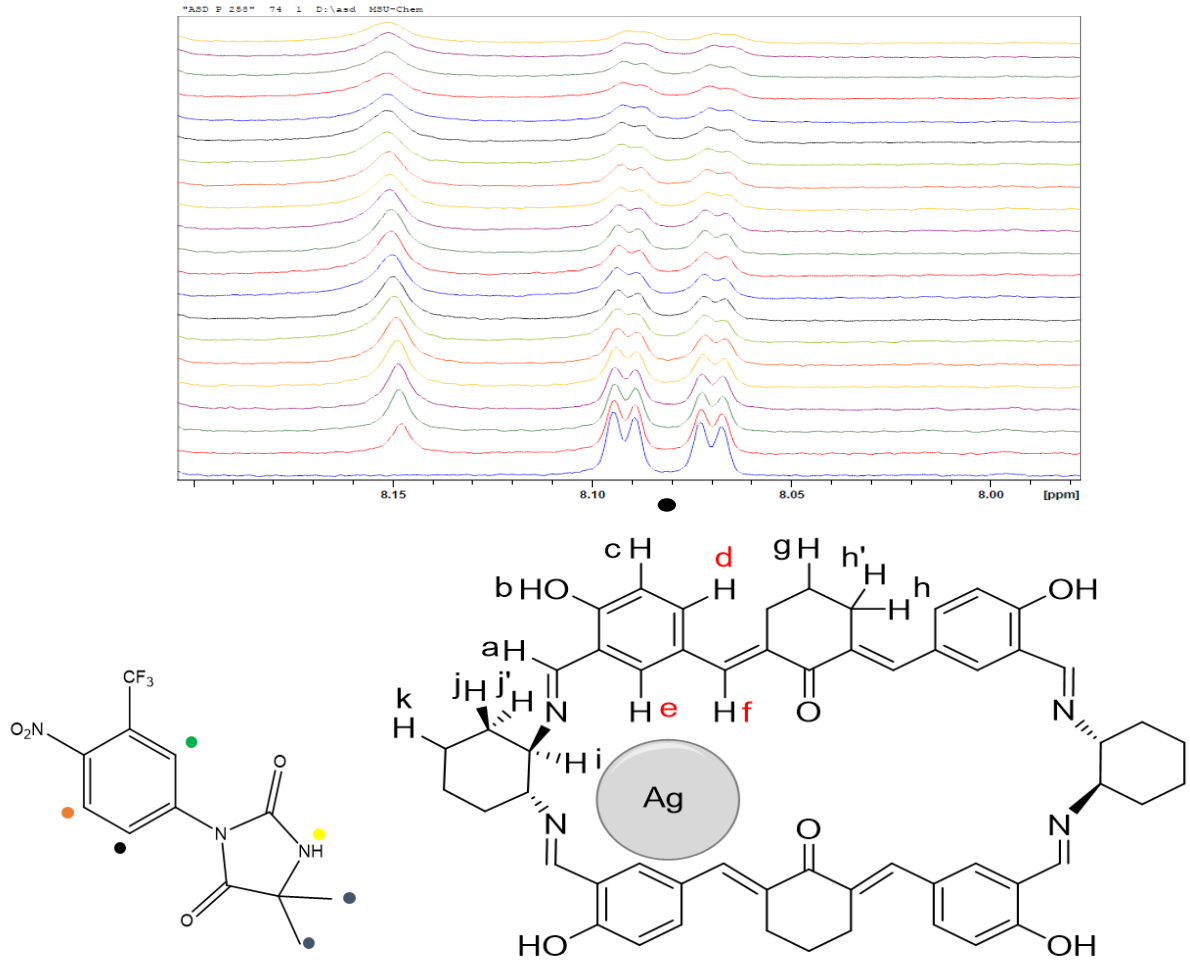

Figure. 2.19. Aromatic proton para to CF_3 group of Nt showed shifting in ^1H NMR titration

The aromatic proton ortho to nitro group of Nt shifted from 8.328 ppm to 8.312 ppm (figure 2.17) while the other aromatic proton ortho to CF_3 group of Nt shifted from 8.215 ppm to 8.212 ppm (figure 2.18). The aromatic proton para to CF_3 group shifted from 8.081 ppm to 8.080 ppm (figure 2.19). This shifting of protons supports the formation of inclusion complex.

The drug loading capacity of the silver corate molecule was found to be 72 % for the drug nilutamide. The encapsulation efficiency of nilutamide was found to be 85 %. To simulate the controlled release of Nt from silver corate, we performed a cumulative release of Nt at two different pH 7.4 (human physiological medium) and pH 5.5 (tumour environment).

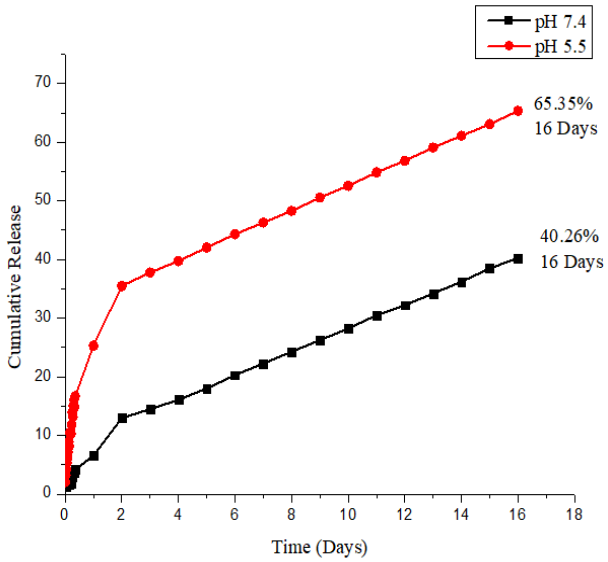

Figure. 2.20. Cumulative release profile of Nilutamide from Silvercorate at pH 7.4 and pH 5.5.

The drug released in two stages. At first stage 12 % of Nt was released in 2 days at pH 7.4 and 25% of Nt was released at pH 5.5 in 2 days (figure 2.20). The controlled release profile of Nt was observed after 2 days up to 16 days at pH 5.5 as well as at pH 7.4. The maximum 65 % of Nt was released up to 16 days in its controlled mode at pH 5.5. This slow diffusion of drug from silvercorate was possible due to the presence of non-covalent interaction between Nt and silvercorate.

The cytotoxicity of tetraiminochiralcorand, nilutamide loaded silver corate and nilutamide were investigated against MDA-MB-231. MDA-MB-231 represents triple negative breast cancer cells which are highly aggressive, invasive and poorly differentiated[69]. The IC_{50} value of tetraiminochiralcorand on MDA-MB-231 was found to be 51.92 µg/ml (table 2.3). Which is slightly higher as compared to anticancer drug Nilutamide which suggest self-therapeutic behaviour of tetraiminochiralcorand. The self–therapeutic behaviour of tetraiminochiralcorand is attributed to the presence of curcuminoid moiety in tetraiminochiralcorand, which keeps its anticancer activity intact.

The cytotoxic activity of inclusion complex of silver corate with Nt was found to be better (IC_{50}= 31.77 µg/ml) than that of free drug Nt (IC_{50}= 38.57 µg/ml). Inclusion complex of combination of drug showed synergistic effect[75] on MDA-MB-231. The enhanced cytotoxicity

of Nt in presence of silver corate is might be due to enhanced cell internalisation followed by sustained release of drug.

Sr. No.	Compound	IC_{50} (MDA-MB-231) (µg/ml)
1.	Tetraiminochiralcorand	51.92 ± 2.53
2.	Silver corate-Nilutamide	31.77 ± 0.8
3.	Nilutamide	38.57 ± 0.45

Table. 2.3. Cytotoxicity of tetraiminochiralcorand, nilutamide loaded silver corate and nilutamide against MDA-MB-231 cancer cells for 24 hours incubation by MTT assay.

B. Encapsulation of cis-platin and dasatinib in tetraiminochiralcorand

We use a kneading approach to encapsulate the cis-platin and dasatinib for an effective combinatorial therapeutic system. The encapsulation is confirmed by the FT-IR spectrum. The drug cis-platin might get bound in the tetraiminochiralcorand due to coordination interaction between two imine and two phenolic groups with platinum (II). The binding causes the stretching band of -C=N to shift from 1627.59 cm^{-1} (spectrum 2.6) to 1630.93 cm^{-1} (spectrum 2.15) and the stretching band of -OH to shift from 3439.39 cm^{-1} (spectrum 2.6) to 3420.77 cm^{-1} (spectrum 2.15).

The encapsulation of dasatinib with tetraiminochiralcorate was also characterized by FT-IR techniques (spectrum 2.16, spectrum 2.17). The encapsulation of drug dasatinib has showed a little effect on the -C=N bond to shift from 1630.93 cm^{-1} (spectrum 2.15) to 1631.36 cm^{-1} (spectrum 2.16). This imine bond shifting demonstrated how dasatinib encapsulation influences the coordination of cis-platin with tetraiminochiralcorand. The shifting in stretching band of alkene group from 1588.80 cm^{-1} to 1583.81 cm^{-1} also supports the active participation of chalcone moiety in encapsulation of dasatinib. The –OH group of aromatic ring is also slightly affected on encapsulation of dasatinib which results in shifting of its stretching band from 3420.77 cm^{-1} (spectrum 2.15) to 3420.24 cm^{-1} (spectrum 2.16). This FT-IR data suggests that the imine and hydroxyl group might take part into the loading of cis-platin while chalcone moiety and aromatic group helps in encapsulation of dasatinib in presence of cis-platin.

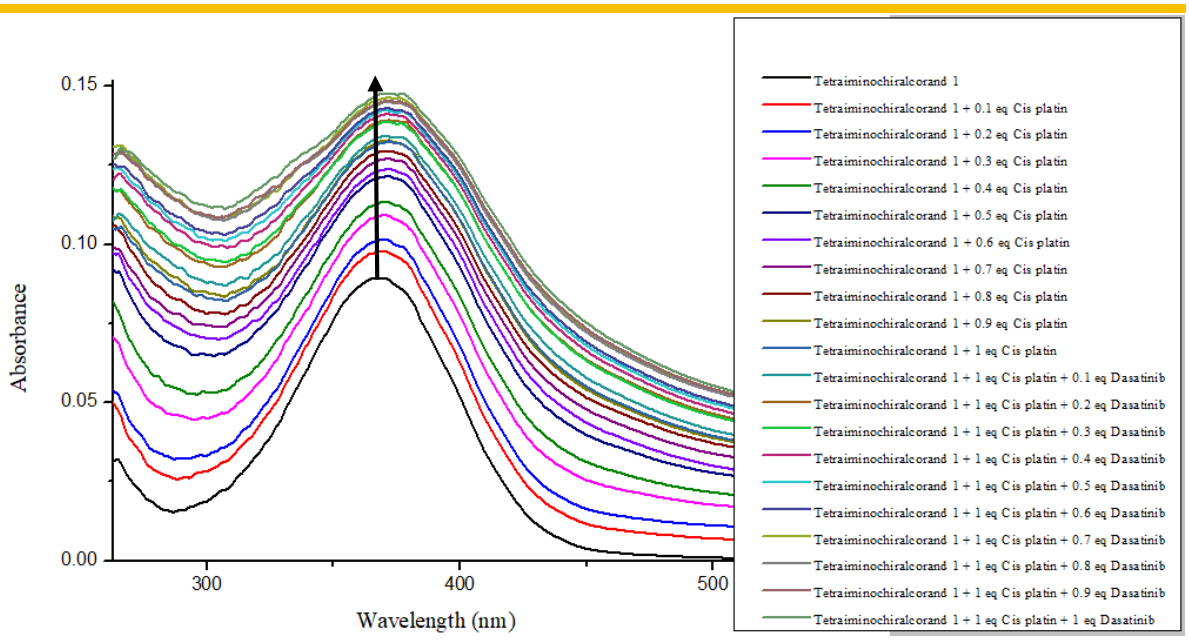

Figure. 2.21. UV-Vis titration of Tetraiminochiralcorand with Cis-platin and Dasatinib

The UV-Vis analysis was conducted to determine the change in absorption peak of corand molecule after the encapsulation of drug. The UV-Vis spectra showed that once the drug was enclosed, there was a slight bathochromic shifting in the absorption peak of tetraiminochiralcorand (figure 2.21). A clear increase in intensity was observed on addition of cis-platin to the tetraiminochiralcorand.

Thermal analysis is a significant technique for recognition and characterisation of drug-carrier complex. Differential scanning calorimetric (DSC) is used for determination of number of phases present in the systems. It is also effective for determining how well a drug interacts with its carrier[74]. As a result, the thermal behaviour of dasatinib, cis-platin, tetraiminochiralcorand, and inclusion complexes were investigated using DSC to characterise the potential of tetraiminochiralcorand for complexation and/or any potential interactions (figure 2.22). Endothermic peaks of drugs and tetraiminochiralcorand are not seen in the DSC thermogram of inclusion complex. It suggests the complete encapsulation of cis-platin and dasatinib within the tetraiminochiralcorand moiety (figure 2.22).

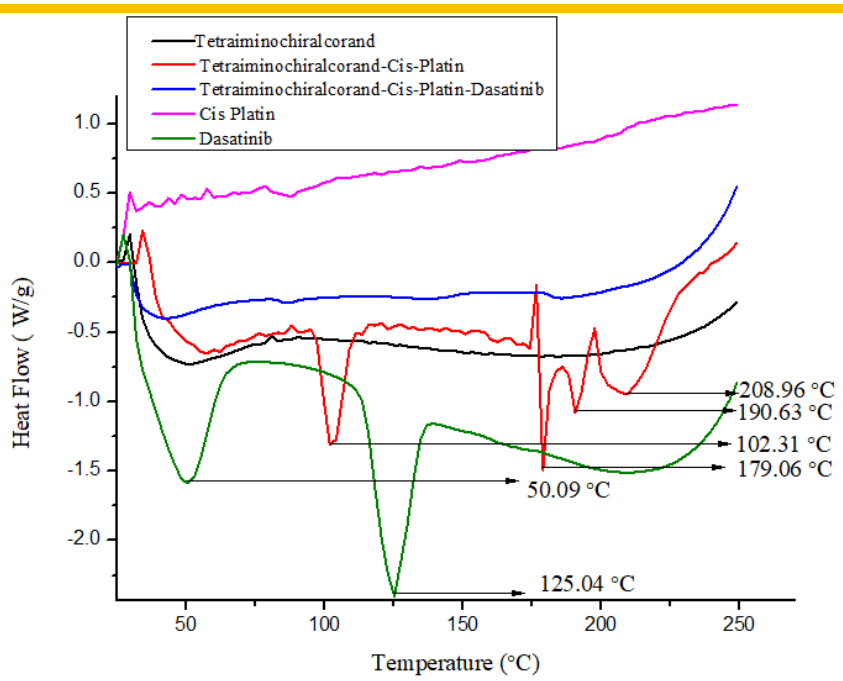

Figure. 2.22. DSC thermogram of Tetraiminochiralcorand, inclusion complexes, Cis-platin, and Dasatinib.

Subsequently, the drug loading capacity of the tetraiminochiralcorate was found to be 73 % for the drug dasatinib. The encapsulation efficiency of dasatinib was found to be 91 %.

The cumulative release experiments of dasatinib were carried out by dialysis method. The release profile of dasatinib was monitored at two different pH 7.4 and 5.5 (figure 2.23). The pH 7.4 mimics the microenvironment of physiological circulation of normal cells and pH 5.5 mimics the microenvironment of cancer cells. The tetraiminochiralcorate molecule showed negligible and slow release of dasatinib at pH 7.4. Approximately there was 4.2 % dasatinib released from tetraiminochiralcorate after 9.5 hours. On the other hand there was rapid release of dasatinib from tetraiminochiralcorate at pH 5.5 compare to pH 7.4. The 28% of dasatinib is initially released in 3.4 hours with a subsequent sustained release of about 48 % within 10 hours. This might be due to acidic environment which reduces the strength of non-covalent interaction between tetraiminochiralcorate, cis-platin and dasatinib. Further, the enhancement in drug release under acidic pH was might be due to the protonation of imine nitrogen which leads to the unavailability of lone pair of nitrogen to bind cis-platin which in turn affects the binding of dasatinib and results in more drug releases at pH 5.5.

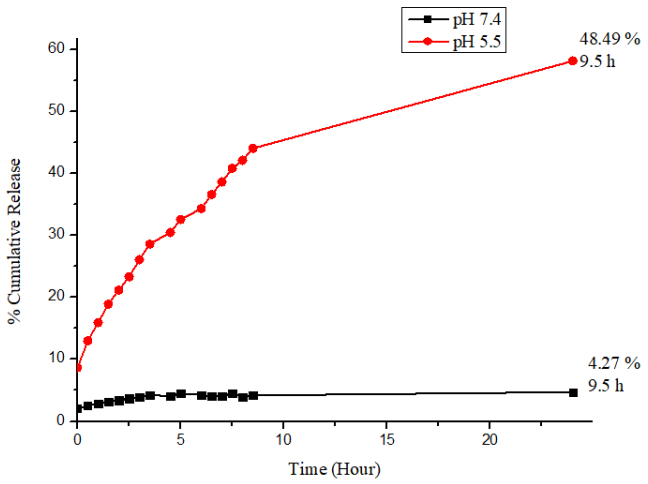

Figure. 2.23. Cumulative release profile of Dasatinib from Cis-platin encapsulated Tetraiminochiralcorand.

The cytotoxic effect of cis-platin, dasatinib and their inclusion complexes with tetraiminochiralcorand on MDA-MB-231 cells was evaluated and their inhibition concentration (IC_{50}) was measured (table 2.4). The IC_{50} values of dasatinib and cis-platin were found to be 32.28 µg/ml and 29.04 µg/ml respectively. The cell treated with inclusion complex of cis-platin and dasatinib with tetraiminochiralcorand has low viability (IC_{50}=20.56 µg/ml) in comparison to free drugs cis-platin and dasatinib which could be related to the capability of internalization of drugs by tetraiminochiralcorand into the cells and releasing the drug in controlled manner. Free drugs can be easily thrown out by drug efflux transporters, which is the only limiting factor in development of efficient chemotherapeutic drug. However, using inclusion complexes of drug with supramolecular carriers overcome the transporter mediated multidrug resistant due to the passing through of supramolecular carriers through the cellular membrane and releasing the drug in a sustained manner[76].

Sr. No.	**Compound**	**IC_{50} (MDA-MB-231) (µg/ml)**
1.	Tetraiminochiralcorand	51.92 ± 2.53
2.	Tetraiminochiralcorand-Cis-Platin	40 ± 1.93
3.	Tetraiminochiralcorand-Cis-Platin-Dasatinib	20.56 ± 1.23
4.	Cis-Platin	29.04 ± 2.93
5.	Dasatinib	32.28 ± 1.37

Table. 2.4. Cytotoxicity of tetraiminochiralcorand, inclusion complexes, cis-platin, and dasatinib against MDA-MB-231 cancer cells for 24 hours incubation by MTT assay.

2.4. Conclusion

We have synthesized a curcuminoid based tetraiminochiralcorand from high dilution method. The SC-XRD analysis showed the definite cavity dimensions of tetraiminochiralcorand which was suitable for the loading of drug in high payload. Two combinatorial systems were developed as follows.

i) Ag^{+} and nilutamide, ii) cis-platin and dasatinib.

Silver being immunomodulator and drug nilutamide known to have anticancer properties were encapsulated in a curcuminoid based tetraiminochiralcorand to develop a combinatorial system with pH triggered and sustained drug release capabilities. The MTT assay against MDA-MB-231 cell line revealed the self-therapeutic behavior of tetraiminochiralcorand. The inclusion complex is found to have enhanced cytotoxic effect on cancerous cells as compared to the free drug nilutamide.

In another combinatorial system cis-platin and dasatinib were chosen. Cis-platin is a potent and versatile anticancer drug but cancer cells develop resistance after a period of time. Dasatinib is known to be used in combination of cis-platin to overcome the resistance of cis-platin. We have encapsulated the combination of drug cis-platin and dasatinib within the tetraiminochiralcorand to achieve a sustained release of drug dasatinib under pH stimulus. The MTT assay against MDA-MB-231 cell line revealed the improved cytotoxic effect on cancerous cells on encapsulation of cis-platin and dasatinib in the tetraiminochiralcorand.

Both the inclusion complexes showed the sustained release of drug under pH stimuli and exhibited better anticancer activity on cancerous cell line suggesting their potential in development of combinatorial chemotherapeutic systems. The inclusion complexes of tetraiminochiralcorand have a strong synergistic cytotoxic effect in both the cases indicating that the overall efficacy improvement might not only be related to the promotion of drug entry into the cells but also to the anti-tumor effect of tetraiminochiralcorand.

2.5 Analytical Data

Spectrum 2.1: ^{1}H NMR spectrum of 2, 6-bis ((E)-4-hydroxybenzylidene)cyclohexan-1-one **DMSO-d$_6$**

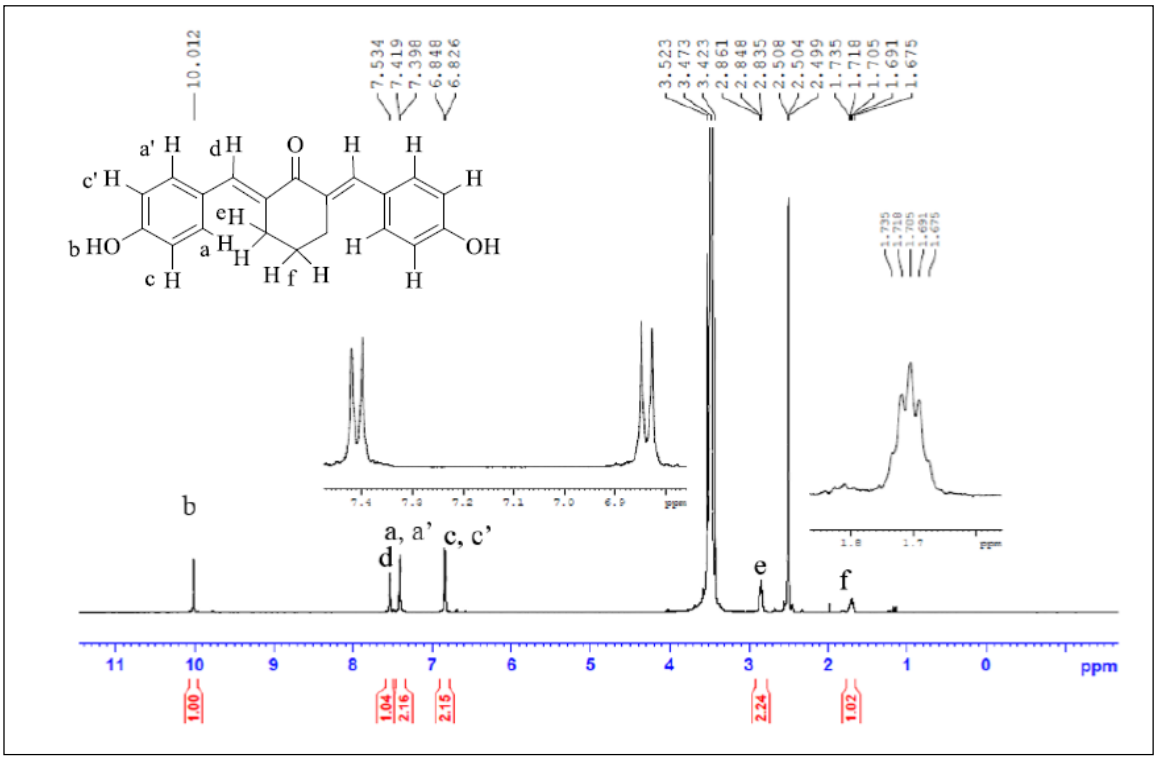

Spectrum 2.2: ^{13}C NMR spectrum of 2, 6-bis ((E)-4-hydroxybenzylidene)cyclohexan-1-one **DMSO-d$_6$**

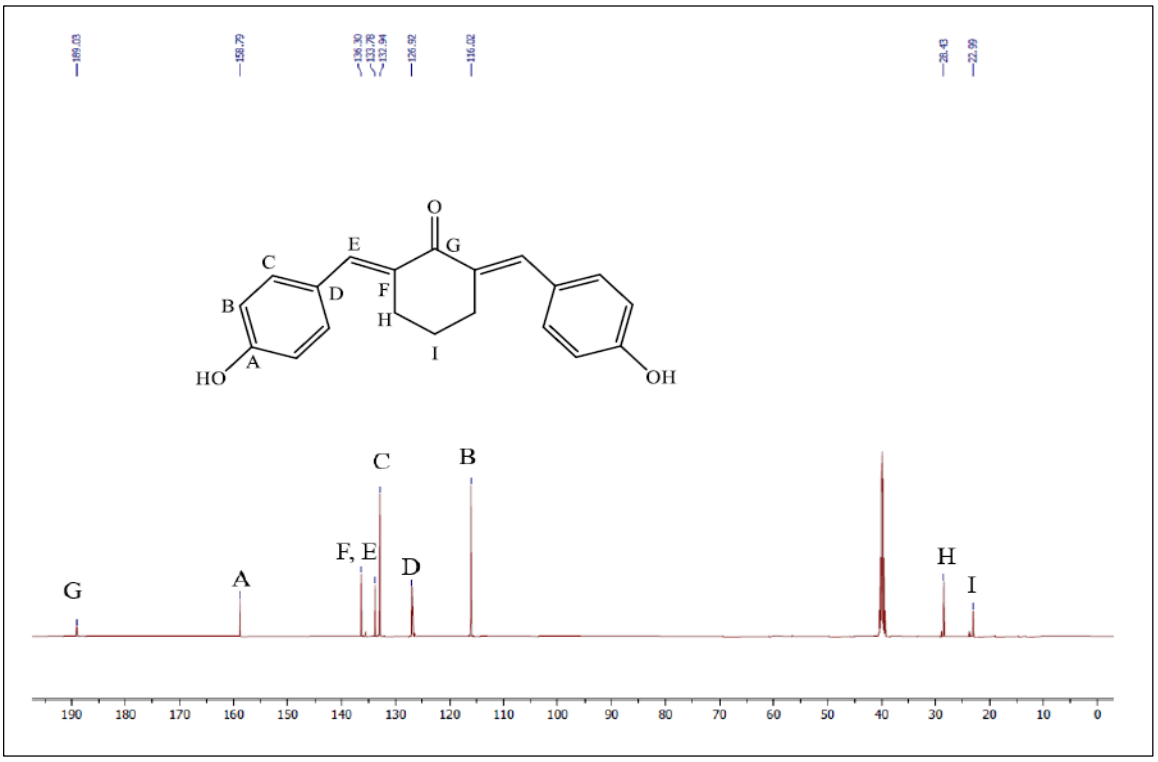

Spectrum 2.3: FT-IR spectrum of 5, 5'-((1E, 1'E)-(2-oxocyclohexane-1, 3-diylidene)bis(methanylylidene))bis(2-hydroxybenzaldehyde)

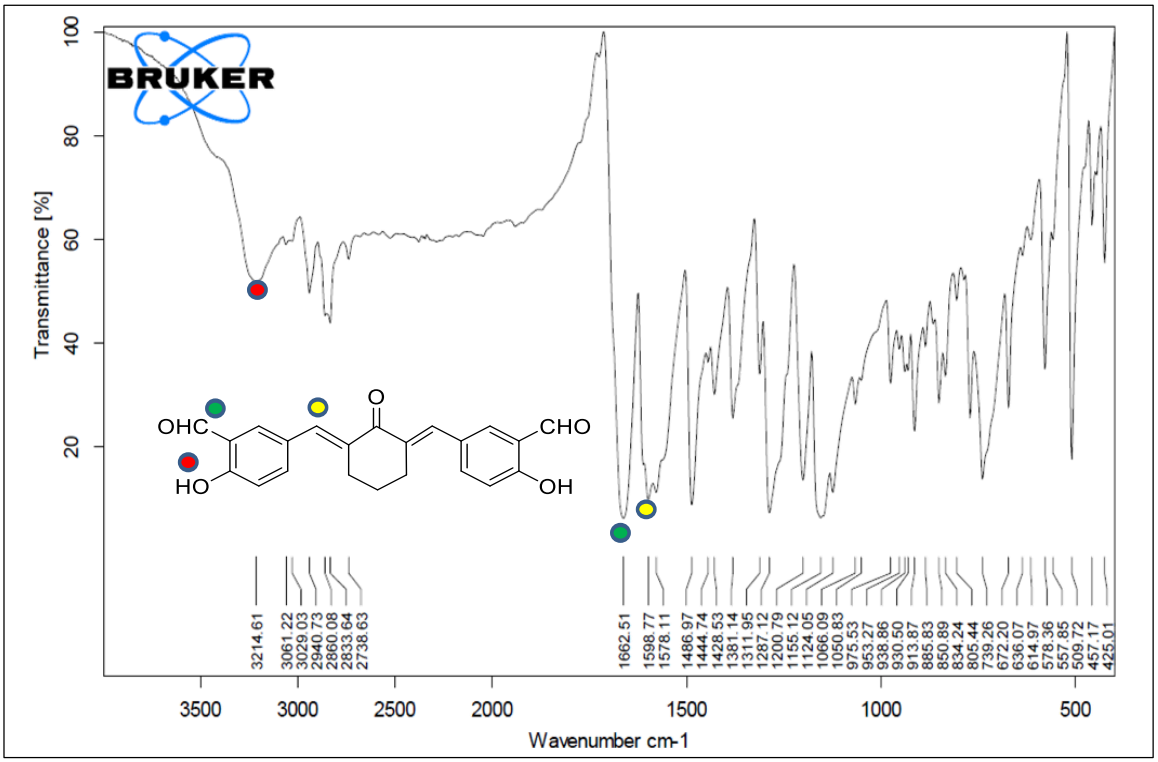

Spectrum 2.4: ^{1}H NMR spectrum of 5, 5'-((1E, 1'E)-(2-oxocyclohexane-1, 3-diylidene)bis(methanylylidene))bis(2-hydroxybenzaldehyde)

$CDCl_3$

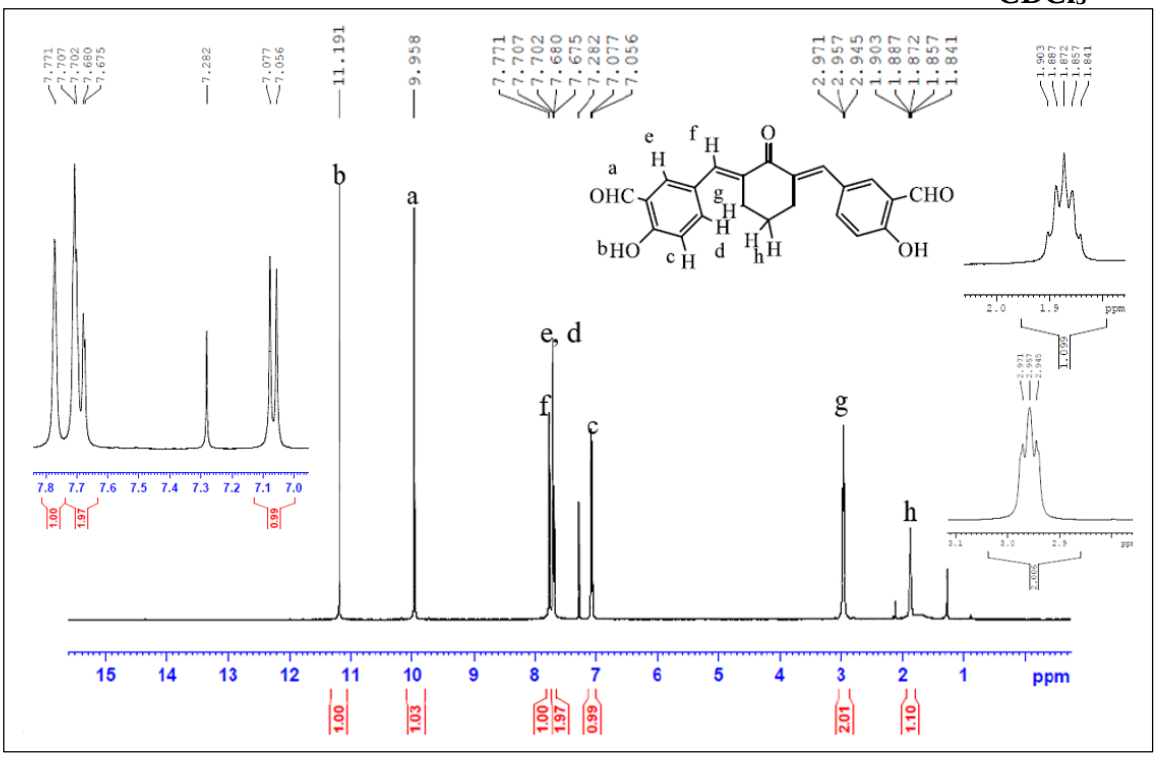

Spectrum 2.5: ^{13}C NMR spectrum of 5, 5'-((1E, 1'E)-(2-oxocyclohexane-1, 3-diylidene)bis(methanylylidene))bis(2-hydroxybenzaldehyde) **$CDCl_3$**

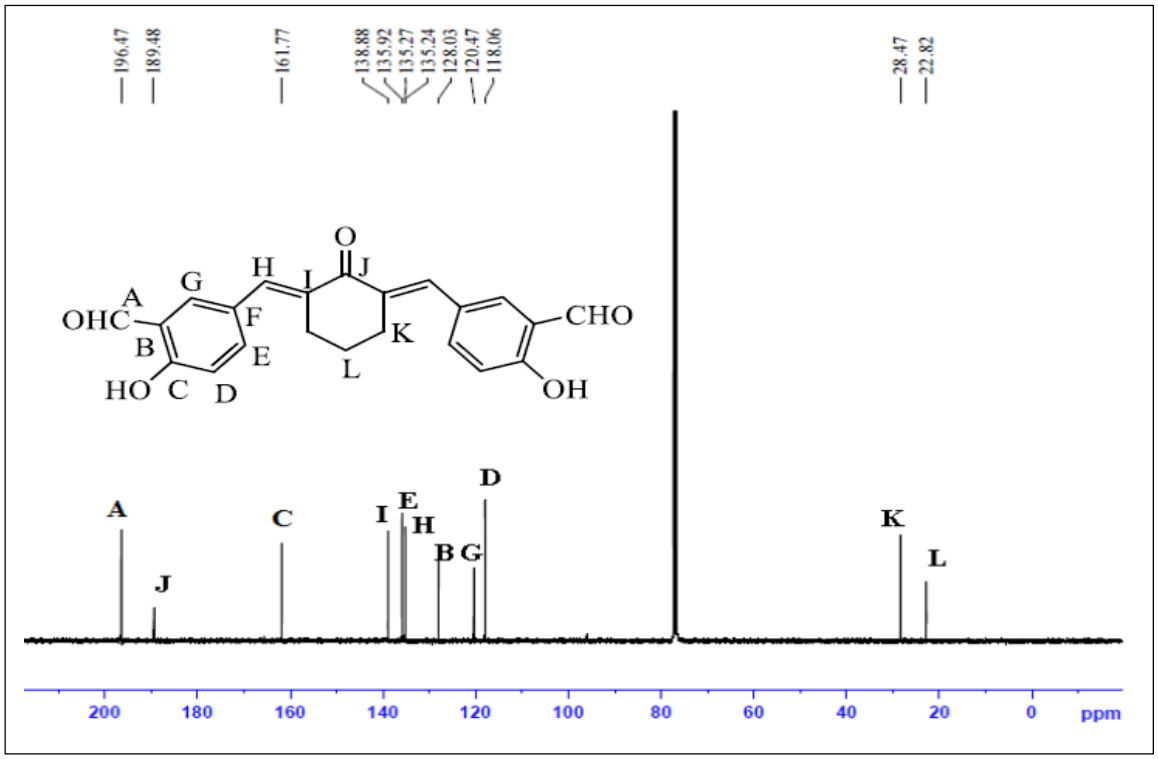

Spectrum 2.6: FT-IR spectrum of tetraiminochiralcorand

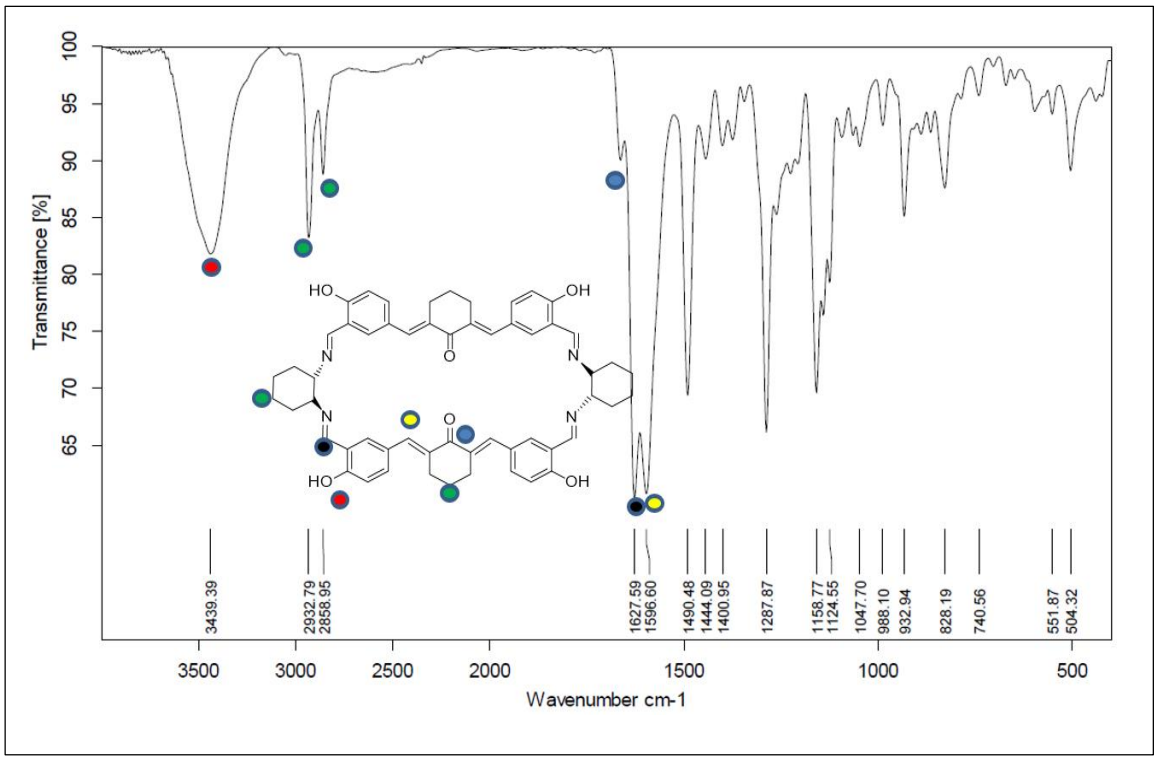

Spectrum 2.7: ^{1}H NMR spectrum of tetraiminochiralcorand

$CDCl_3$

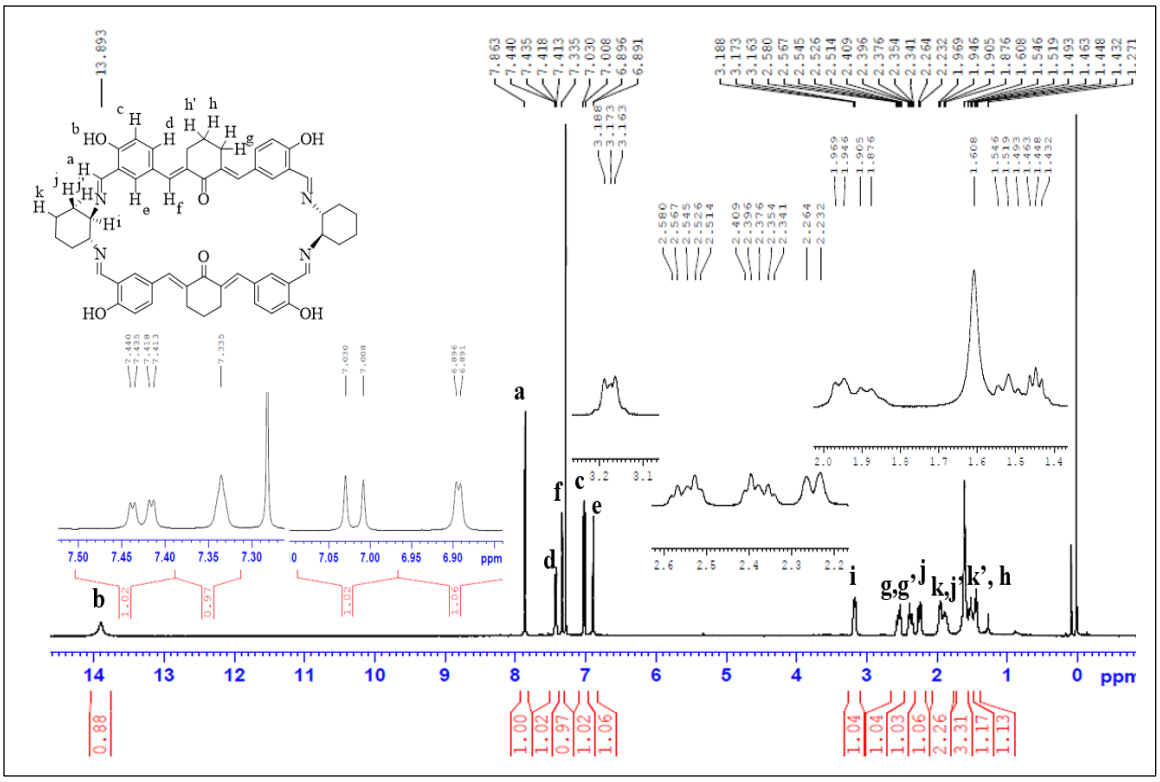

Spectrum 2.8: ^{13}C NMR spectrum of tetraiminochiralcorand

$CDCl_3$

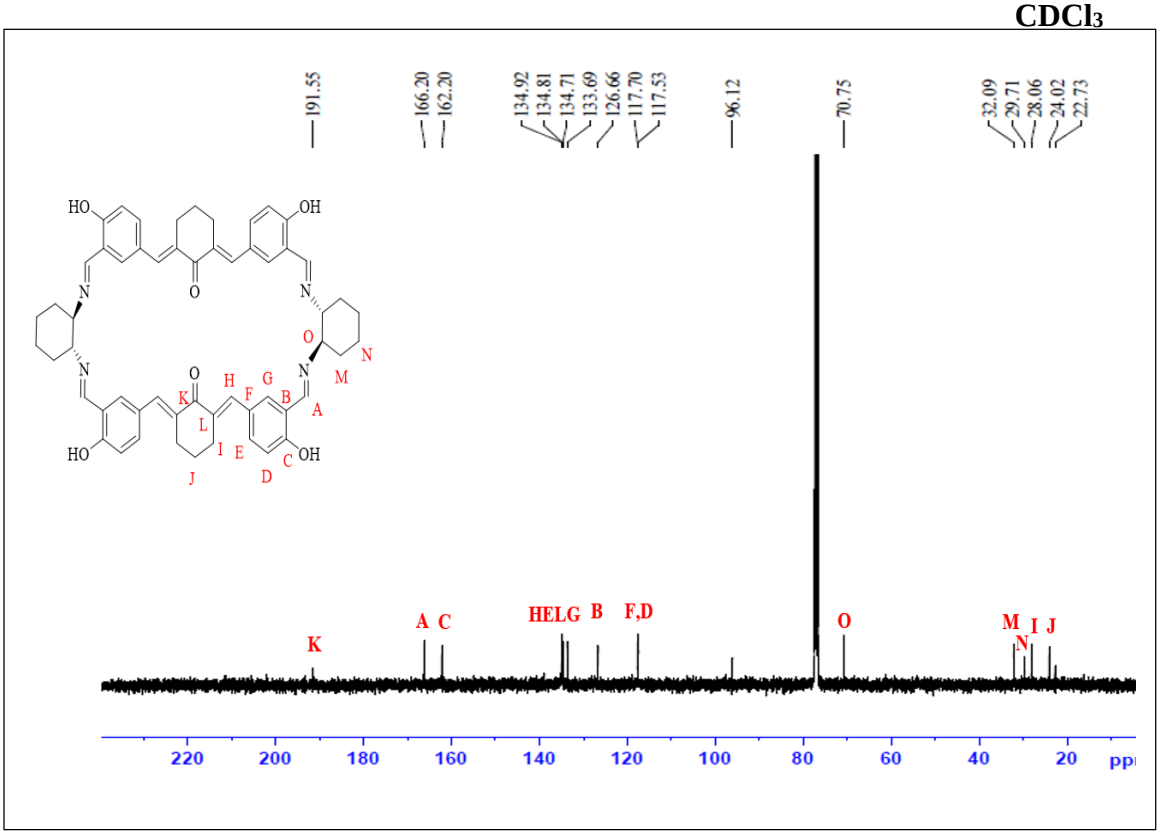

Spectrum 2.9: 135 DEPT NMR spectrum of tetraiminochiralcorand

$CDCl_3$

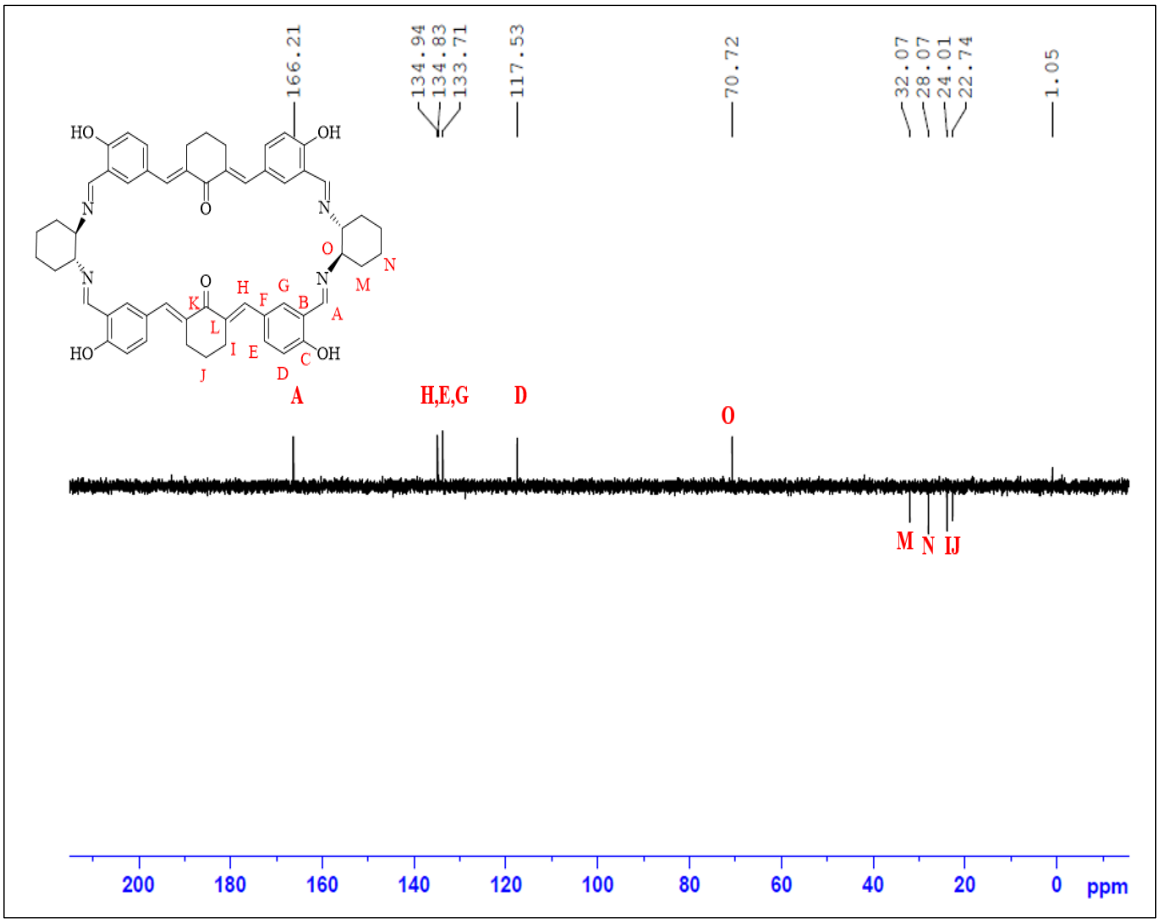

Spectrum 2.10: HR-MS spectrum of tetraiminochiralcorand

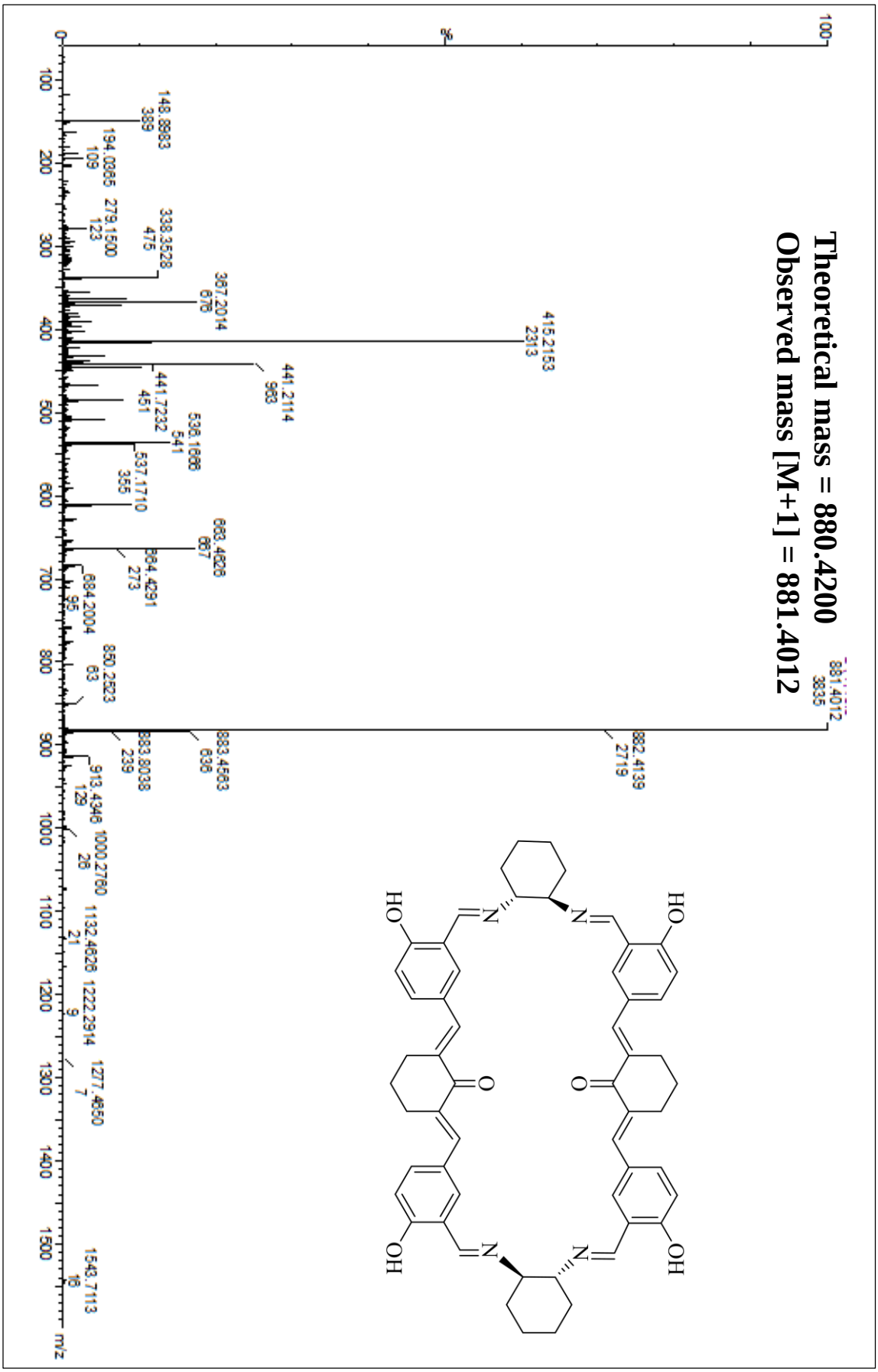

Spectrum 2.11: FT-IR spectrum of Silver-corate

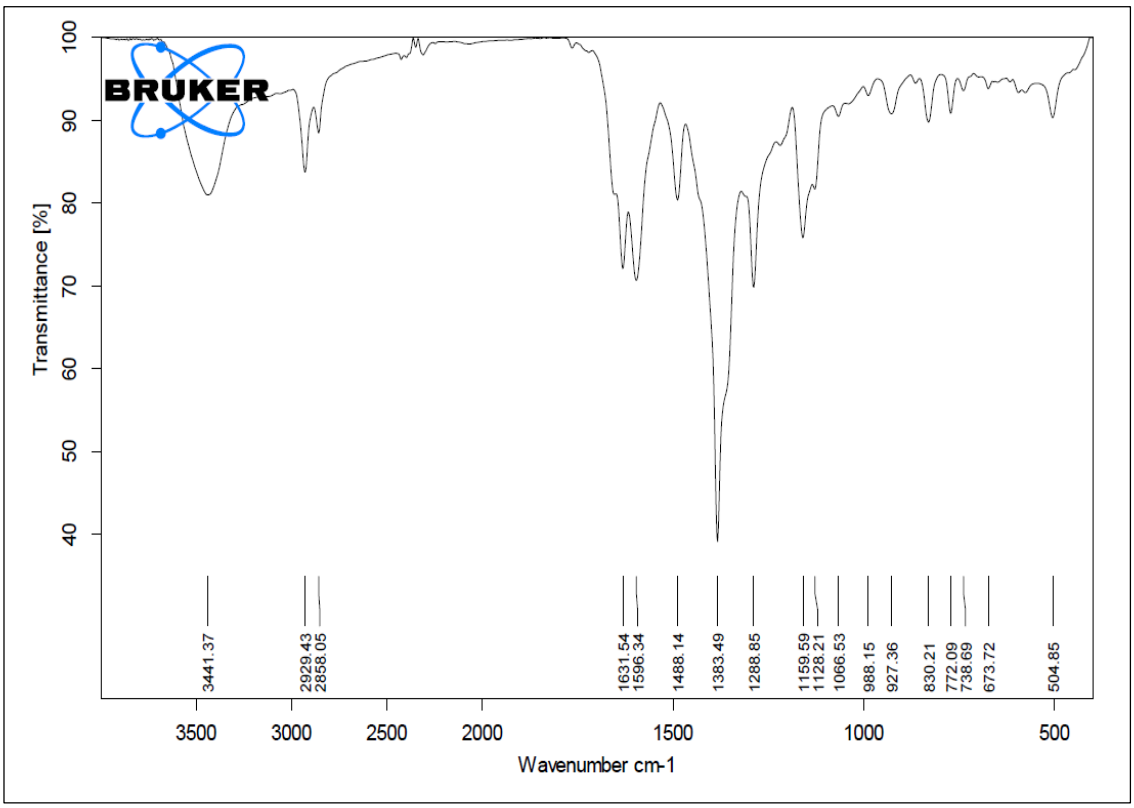

Spectrum 2.12: FT-IR spectrum of Nilutamide loaded Silvercorate

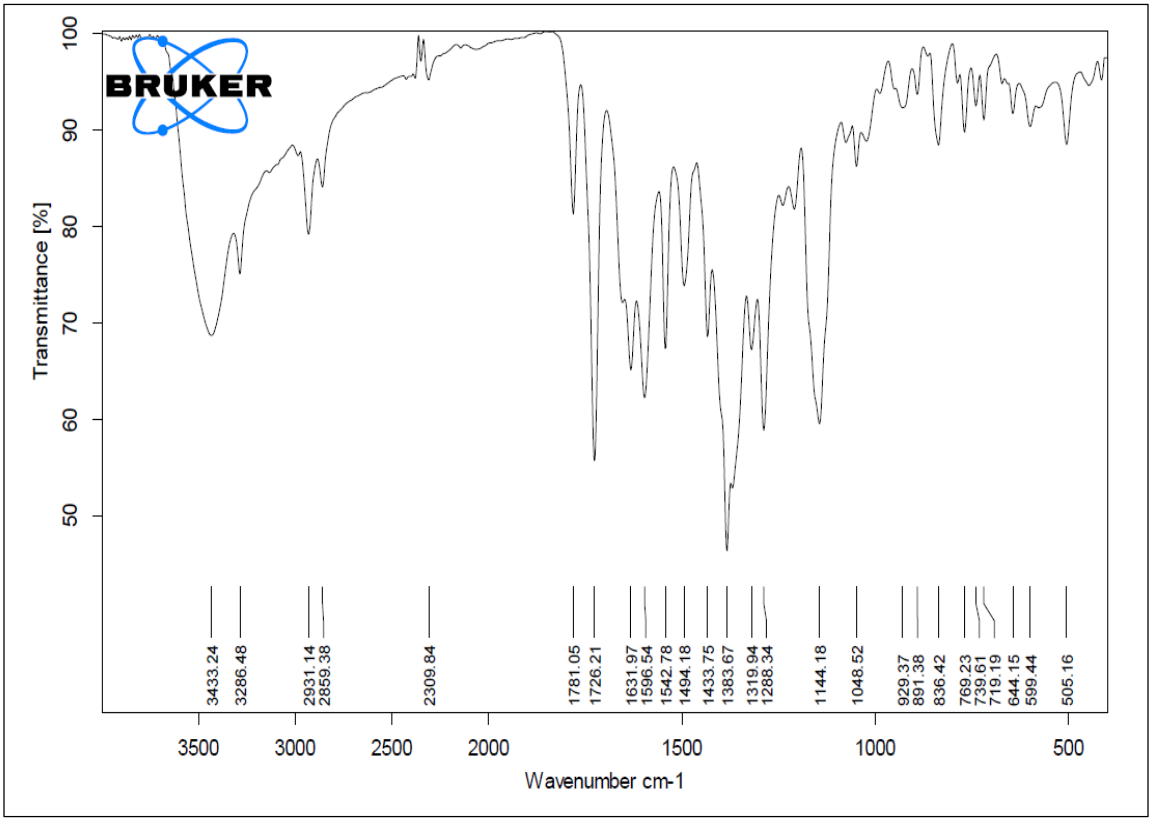

Spectrum 2.13: FT-IR spectrum of Nilutamide

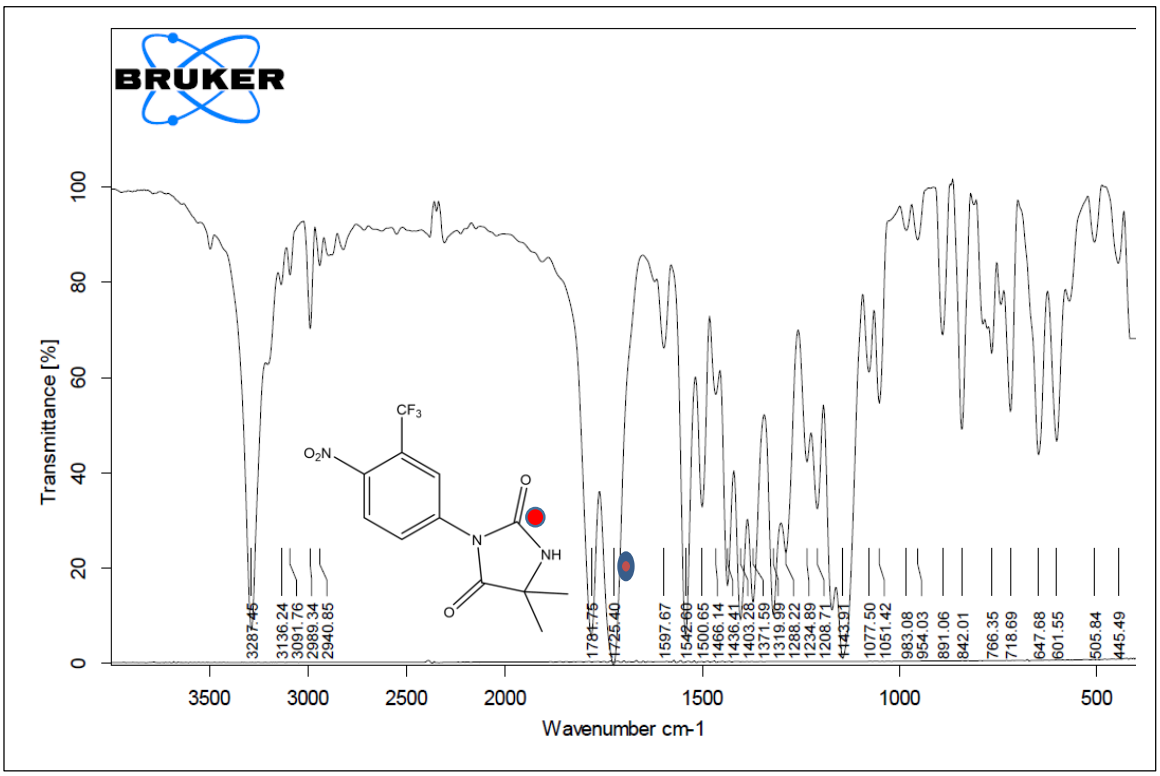

Spectrum 2.14: ^{1}H NMR spectrum of Nilutamide

DMSO-d$_6$

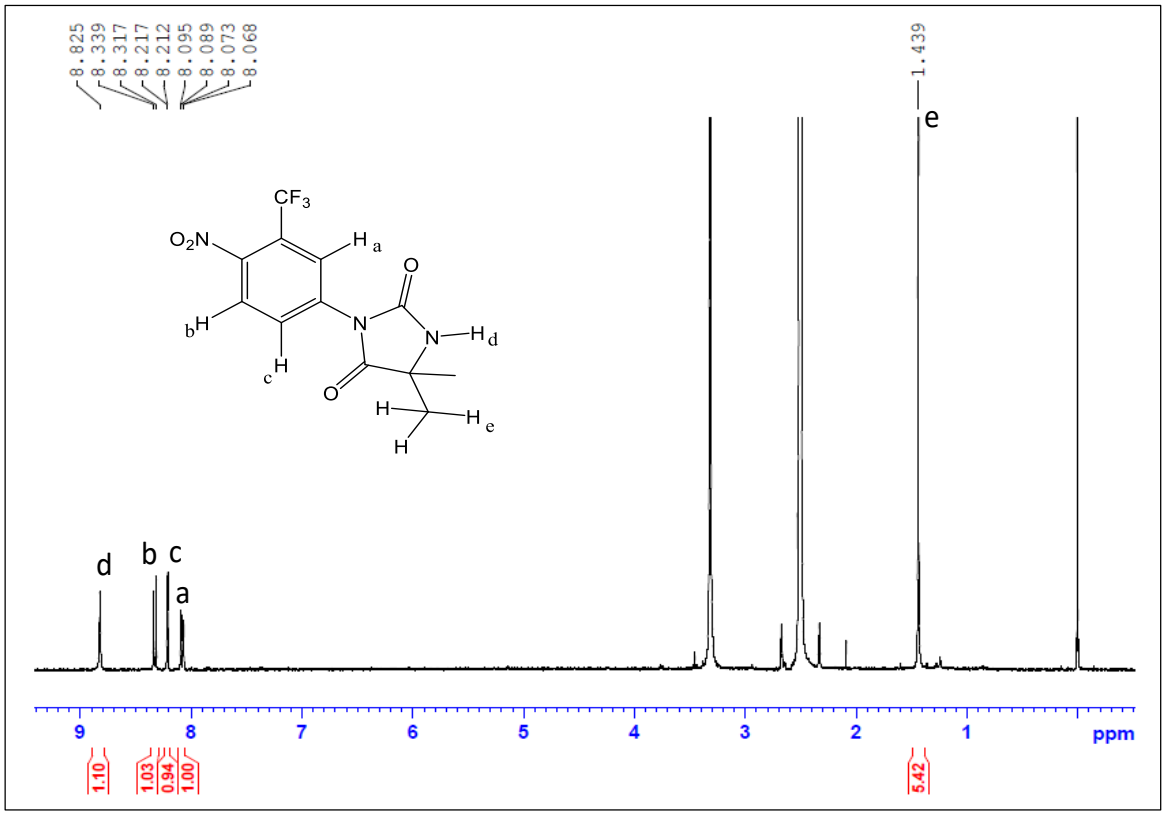

Spectrum 2.15: FT-IR spectrum of Cis-platin loaded tetraiminochiralcorand

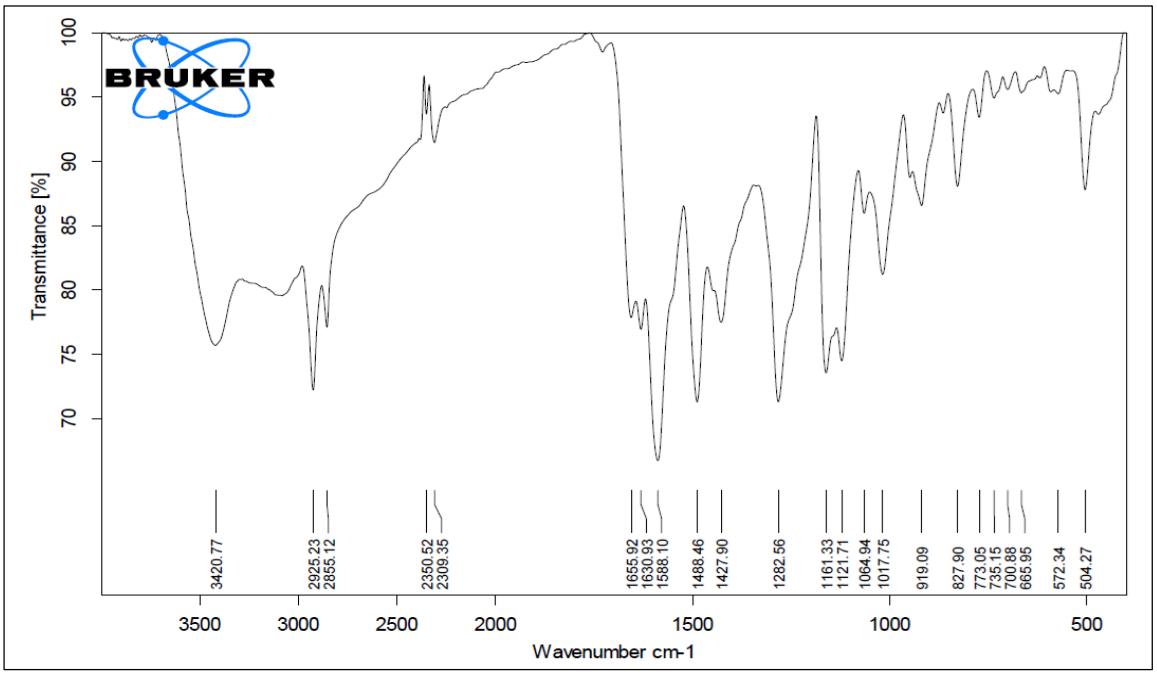

Spectrum 2.16: FT-IR spectrum of Dasatinib and Cis-platin loaded tetraiminochiralcorand

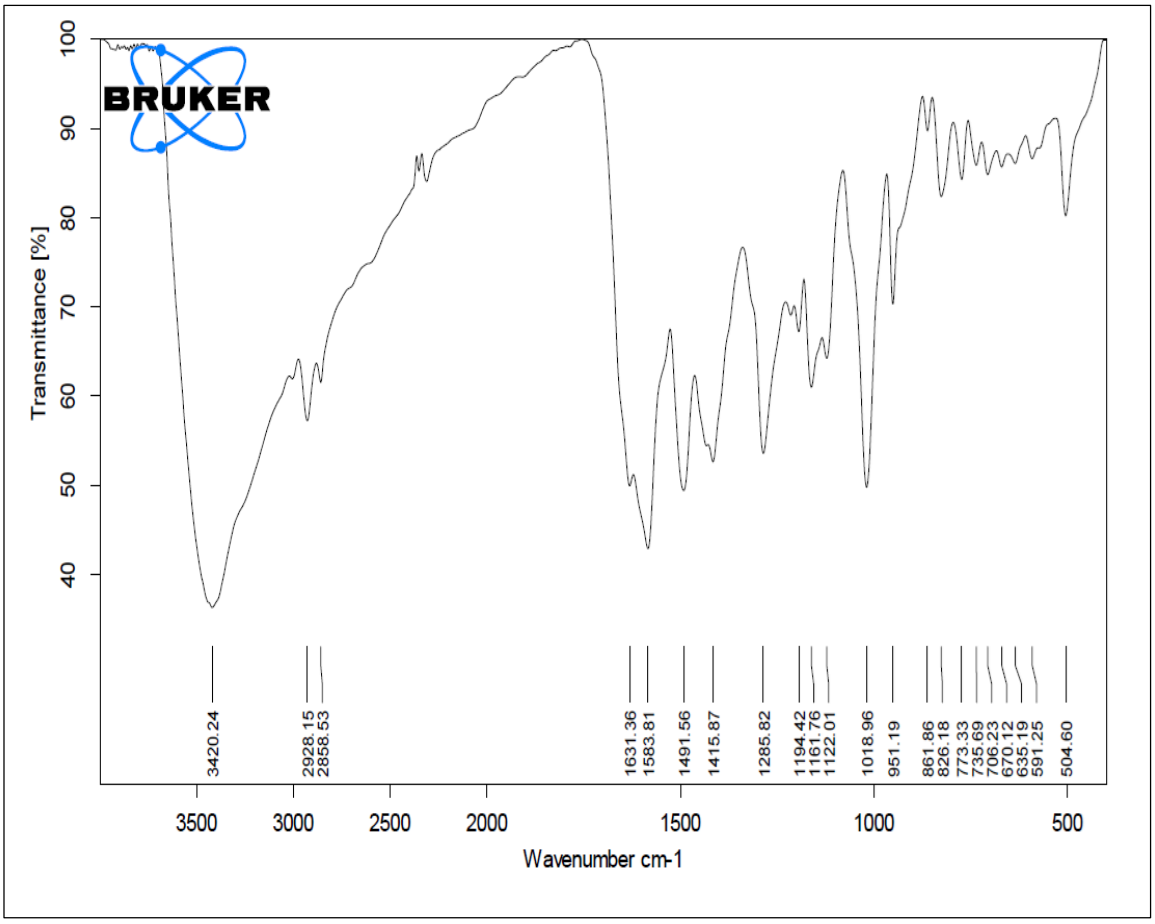

Spectrum 2.17: FT-IR spectrum of Dasatinib

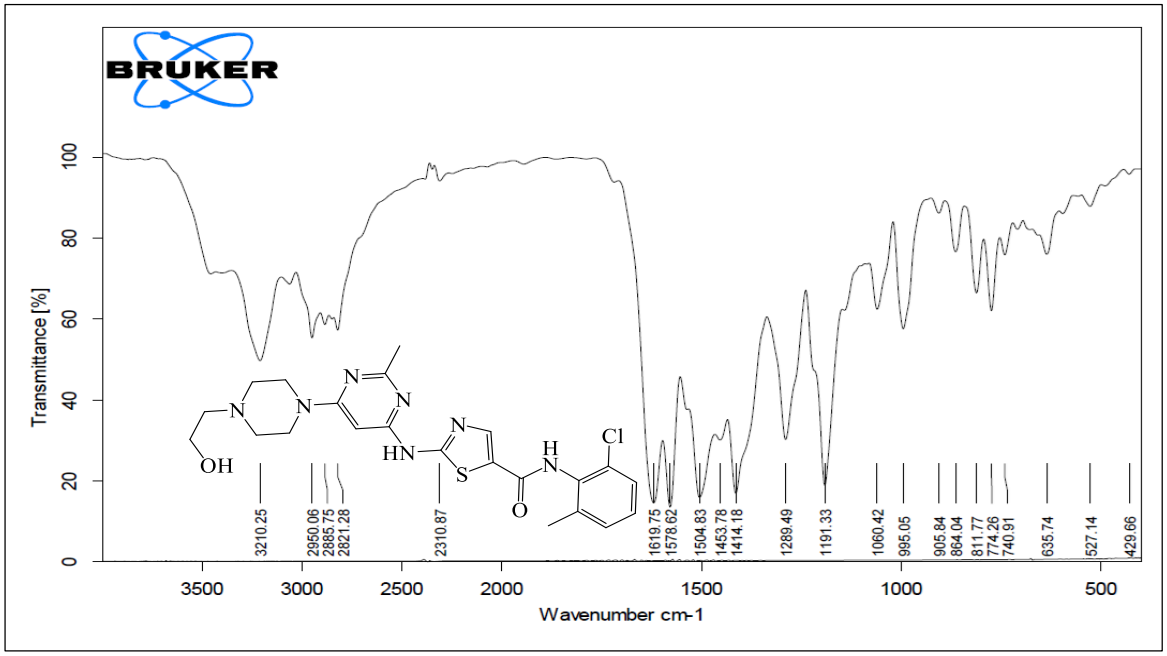

2.6. References

1 W. Feng, M. Jin, K. Yang, Y. Pei, Z. Pei, *Chem. Commun.*, 2018, **54**, 13626–13640.

2 M. J. Webber, R. Langer, *Chem. Soc. Rev.*, 2017, **46**, 6600–6620.

3 A. Mokhtarzadeh, S. Hassanpour, Z. F. Vahid, M. Hejazi, M. Hashemi, J. Ranjbari, M. Tabarzad, S. Noorolyai, M. D. Guardia, *J. Control. Release*, 2017, **266**, 166-186.

4 W. H. Brooks, W. C. Guida, K. G. Daniel, *Curr. Top. Med. Chem.*, 2011, **11**, 760–770.

5 J. Yeom, P. P. G. Guimaraes, H. M. Ahn, B. Jung, Q. Hu, K. Mchugh, M. J. Mitchell, C. Yun, R. Langer, A. Jaklenec, *Adv. Mater.*, 2019, **32**, 1–10.

6 R. Jayakumar, R. Vadivel, N. Ananthi, *Org. Med. Chem.*, 2018, **5,** 1-6.

7 J. Deng, S. Wu, M. Yao, C. Gao, *Sci. Rep.*, 2016, **6,** 31595.

8 L. Yuan, F. Zhang, X. Qi, Y. Yang, C. Yan, J. Jiang, J. Deng, *J. Nanobiotechnolo.*, 2018, **16**, 1–16.

9 X. Yao, Y. Hu, B. Cao, R. Peng, J. Ding, *Biomaterials*, 2013, **34**, 9001-9009.

10 J. Deng, H. Zheng, X. Zheng, M. Yao, Z. Li, C. Gao, *Nano Res.*, 2016, **9**, 3683–3694.

11 X. Wang, H. Gan, T. Sun, *Adv. Funct. Mater.*, 2011, **21**, 3276–3281.

12 J. Deng, Z. Li, M. Yao, C. Gao, *Langmuir*, 2016, **32**, 5608-5616.

13 J. Deng, M. Yao, C. Gao, *Acta Biomater.*, 2017, **53**, 610-618.

14 L. Song, M. Pan, R. Zhao, J. Deng, Y. Wu, *J. Control. Release*, 2020, **324**, 156-171.

15 Z. Li, C. Jablonski, *Inorg. Chem.*, 2000, **39**, 2456–2461.

16 H. Shimakoshi, H. Takemoto, I. Aritome, Y. Hisaeda, *Tetrahedron Lett.*, 2002, **43**, 4809–4812.

17 H. Shimakoshi, T. Kai, I. Aritome, Y. Hisaeda, *Tetrahedron Lett.*, 2002, **43**, 8261–8264.

18 S. Srimurugan, B. Viswanathan, T. K. Varadarajan, B. Varghese, *Tetrahedron Lett.*, 2005, **46**, 3151–3155.

19 S. Srimurugan, B. Viswanathan, T. K. Varadarajan, B. Varghese, *Org. Biomol. Chem.*,

2006, **4**, 3044–3047.

20 S. R. Korupoju, N. Mangayarkarasi, S. Ameerunisha, E. J. Valente, P. S. Zacharias, *J. Chem. Soc. Dalt. Trans.*, 2000, 2845–2852.

21 M. Kwit, J. Gawronski, *Tetrahedron Asymmetry*, 2003, **14**, 1303–1308.

22 M. Paluch, J. Lisowski, T. Lis, *Dalton Trans.*, 2006, 381–388.

23 K. Tanaka, T. Tsuchitani, N. Fukuda, A. Masumoto, R. Arakawa, *Tetrahedron Asymmetry*, 2012, **23**, 205–208.

24 K. Tanaka, N. Fukuda, *Tetrahedron Asymmetry*, 2009, **20**, 111–114.

25 K. Tanaka, R. Shimoura, M. R. Caira, *Tetrahedron Lett.*, 2010, **51**, 449–452.

26 J. Gawronski, H. Kołbon, M. Kwit, A. Katrusiak, *J. Org. Chem.*, 2000, **65**, 5768–5773.

27 M. Kwit, P. Skowronek, H. Kołbon, J. Gawroński, *Chirality*, 2005, **17**, 93–100.

28 J. Gawronski, K. Gawronska, J. Grajewski, M. Kwit, A. Plutecka, U. Rychlewska, *Chem. Eur. J.*, 2006, **12**, 1807–1817.

29 J. Gregolinski, J. lisowski, T. Lis, *Org. Biomol. Chem.*, 2005, **3**, 3161-3166.

30 M. Chadim, M. Budesinsky, J. Hodacova, J. Zavada, P. C. Junk, *Tetrahedron Asymmetry*, 2001, **12**, 127–133.

31 J. Gao, A. E. Martell, *Org. Biomol. Chem.*, 2003, **1**, 2795–2800.

32 J. Hodacova, M. Chadim, J. Zavada, J. Aguilar, E. Garcia-Espana, S. V. Luis, J. F. Miravet, *J. Org. Chem.*, 2005, **70**, 2042–2047.

33 C. Ma, A. Lo, A. Abdolmaleki, M. J. MacLachlan, *Org. Lett.*, 2004, **6**, 3841–3844.

34 N. Kuhnert, G. M. Rossignolo, A. L. Periago, *Org. Biomol. Chem.*, 2003, **1**, 1157–1170.

35 N. Kuhnert, A. M. L. Periago, *Tetrahedron Lett.*, 2002, **43**, 3329–3332.

36 N. Kuhnert, C. Straßnig, A. M. L. Periago, *Tetrahedron Asymmetry*, 2002, **13**, 123–128.

37 N. Kuhnert, A. L. Periago, G. M. Rossignolo, *Org. Biomol. Chem.*, 2005, **3**, 524–537.

38 N. Kuhnert, C. Patel, F. Jami, *Tetrahedron Lett.*, 2005, **46**, 7575–7579.

39 N. Kuhnert, N. Burzlaff, C. Patel, A. L. Periago, *Org. Biomol. Chem.*, 2005, **3**, 1911–1921.

40 J. Gao, A. E. Martell, *Org. Biomol. Chem.*, 2003, **1**, 2801–2806.

41 J. Lin, H. C. Zhang, L. Pu, *Org. Lett.*, 2002, **4**, 3297–3300.

42 Z. B. Li, J. Lin, M. Sabat, M. Hyacinth, L. Pu, *J. Org. Chem.*, 2007, **72**, 4905–4916.

43 M. Petryk, A. Janiak, L. J. Barbour, M. Kwit, *Eur. J. Org. Chem.*, 2018, **2018**, 1916-1923.

44 J. Szymkowiak, B. Warzajtis, U. Rychlewska, M. Kwit, *Chem. Eur. J.*, 2018, **24**, 6041-6046.

45 J. Szymkowiak, B. Warzajtis, U. Rychlewska, M. Kwit, *Cryst. Eng. Chem.*, 2018, **20**, 5200-5208.

46 T. Packowski, J. Gregolinski, K. Slepokura, J. Lisowski, *Tetrahedron Lett.*, 2018, **59**, 3669-3673.

47 R. Frydrych, K. Slepokura, A. Bil, J. Gregolinski, *J. Org. Chem.*, 2019, **84**, 5695-5711.

48 M. Zgorzelak, J. Grajewski, *J. Mol. Struct.*, 2020, **1202**, 127336.

49 M. Zgorzelak, J. Grajewski, J. Gawronski, M. Kwit, *Chem. Commun.*, 2019, **55**, 2301-2304.

50 D. Fedorowicz, S. Banach, P. Koza, R. Frydrych, K. Slepokura, J. Gregolinski, *Org. Biomol. Chem.*, 2022, **20**, 1080-1094.

51 A. Janiak, J. Gajewy, J. Szymkowiak, B. Gierczyk, M. Kwit, *J. Org. Chem.*, 2022, **87**, 2356-2366.

52 A. S. Desai, T. Rajamannar, S. R. Shah, *ChemistrySelect*, 2020, **5**, 10588–10592.

53 L. Song, M. Pan, R. Zhao, J. Deng, Y. Wu, *J. Control. Release*, 2020, **324**, 156–171.

54 S. Tripathy, D. K. Verma, M. Thakur, A. R. Patel, P. P. Srivastav, S. Singh, A. K. Gupta, M. L. Chávez-González, C. N. Aguilar, N. Chakravorty, H. K. Verma, G. L. Utama, *Front. Nutr.*, 2021, 8, 747966.

55 W. H. Talib, S. A. A. Hadid, M. B. W. Ali, I. H. A. Yasari, M. R. A. Ali, *Breast Cancer Targets Ther.*, 2018, **10**, 207–217.

56 M. A. Tomeh, R. Hadianamrei, X. Zhao, *Int. J. Mol. Sci.*, 2019, **20**, 1-26.

57 L. Friedman, L. Lin, S. Ball, T. Bekaii-Saab, J. Fuchs, P. K. Li, C. Li and J. Lin, *Anticancer Drugs*, 2009, **20**, 444–449.

58 L. Lin, B. Hutzen, S. Ball, E. Foust, M. Sobo, S. Deangelis, B. Pandit, L. Friedman, C. Li, P. K. Li, J. Fuchs, J. Lin, *Cancer Sci.*, 2009, **100**, 1719–1727.

59 J. R. Fuchs, B. Pandit, D. Bhasin, J. P. Etter, N. Regan, D. Abdelhamid, C. Li, J. Lin, P. K. Li, *Bioorganic Med. Chem. Lett.*, 2009, **19**, 2065–2069.

60 S. Mapoung, S. Suzuki, S. Fuji, A. Naiki-Ito, H. Kato, S. Yodkeeree, C. Ovatlarnporn, S. Takahashi, P. Limtrakul, *Cancer Sci.*, 2019, **110**, 596–607.

61 H. Ohori, H. Yamakoshi, M. Tomizawa, M. Shibuya, Y. Kakudo, A. Takahashi, S. Takahashi, S. Kato, T. Suzuki, C. Ishioka, Y. Iwabuchi, H. Shibata, *Mol. Cancer Ther.*, 2006, **5**, 2563–2571.

62 I. Huber, E. Pandur, K. Sipos, L. Barna, A. Harazin, M. A. Deli, L. Tyukodi, G. G. Fekete, G. Kulcsar, Z. Rozmer, *Eur. J. Pharm. Sci.*, 2022, 173, 106184

63 A. Thakur, S. Manohar, C. E. Velez Gerena, B. Zayas, V. Kumar, S. V. Malhotra and D. S. Rawat, *Med. chem. commun.*, 2014, **5**, 576–586.

64 S. W. Leong, T. Awin, S. M. Mohd Faudzi, M. Maulidiani, K. Shaari, F. Abas, *Med. Chem. Res.*, 2019, **28**, 2002–2009.

65 P. Mathur, M. Mori, H. Vyas, K. Mor, J. Jagtap, S. Vadher, K. Vyas, R. Devkar, A. Desai, *ACS Omega*, 2022, **7**, 45545–45555.

66 A. Desai, P. Mathur, A novel class of supramolecular compounds: compound of formula (IA) and (IB). Indian Patent 369055, 2021. https://patentscope.wipo.int/search/en/detail.jsf?ocId=IN335044831&_cid=P12-L40W51-74422-2.

67 A. Desai, P. Mathur, Novel bis (hydroxy benzylidene) cyclic ketone based tetra-aza corand.

Indianpatent.369745,2021.https://patentscope.wipo.int/search/en/detail.jsf?docId=IN335044831&_cid=P10-KZQKS6- 63174-1.

68 A. Desai, P. Mathur, Novel bis (hydroxy benzylidene) cyclic ketone based tetra-aza corand. US patent application 17/639,918.

69 S. A. Sabra, S. A. Sheweita, M. Haroun, D. Ragab, M. A. Eldemellawy, Y. Xia, D. Goodale, A. L. Allan, A. O. Elzoghby, S. Rohani, *J. Pharm. Sci.*, 2019, **108**, 1713–1725.

70 O. V. Dolomanov, L. J. Bourhis, R. J. Gildea, J. A. K. Howard, H. Puschmann, *J. Appl. Crystallogr.*, 2009, **42**, 339–341.

71 G. M. Sheldrick, *Acta Crystallogr. Sect. A Found. Crystallogr.*, 2008, **A64**, 112–122.

72 R. F. V. Macias, S. A. Patino, R. C. Betancourt, I. R. Esquivel, G. F. Reyes, N. C. Gonzalez, *Rev. Mex. Urol.*, 2016, **76**, 346-351.

73 C. M. Venema, R. D. Bense, T. G. steenbruggen, H. H. Nienhuis, S. Q. Qiu, M. V. Kruchten, M. Brown, R. M. Tamimi, G. A. P. Hospers, C. P. Schroder, R. S. N. Fehrmann, E. G. D. Vries, *Pharmacol. Ther.*, 2019, **200**, 135-147.

74 T. A. A. Hujran, M. K. Magharbeh, S. A. gharabli, R. R. Haddadin, M. N. A. Soub, H. M. Tawfeek, *Pharmaceutics*, 2021, **13**, 1-16 .

75 L. An, J. Wang, J. Liu, Z. Zhao, Y. Song, Front. Chem., 2019, 7, 1-14.

76 M. Rahimi, R. Karimian, E. B. Noruzi, K. Ganbarov, M. Zarei, F. S. Kamounah, B. Yousefi, M. Bastami, M. Yousefi, H. S. Kafil, *Int. J. Nanomed.*, 2019, **14**, 2619-2636.